THIN FILM PIEZOELECTRIC ON SUBSTRATE RESONATORS ELECTRICAL CHARACTERIZATION AND OSCILLATOR CIRCUIT DESIGN

By

DERYA DIKBAS

Bachelor of Science in Electrical Engineering

Istanbul Yildiz Technical University

Istanbul, Turkey

2009

Submitted to the Faculty of the
Graduate College of the
Oklahoma State University
in partial fulfillment of
the requirements for
the Degree of
MASTER OF SCIENCE
December, 2011

THIN FILM PIEZOELECTRIC ON SUBSTRATE

RESONATORS ELECTRICAL CHARACTERIZATION

AND

OSCILLATOR CIRCUIT DESIGN

Thesis Approved:

Dr. Reza Abdolvand

Thesis Adviser

Dr. John M. Acken

Dr. Kenneth F. Ede

Dr. Sheryl A. Tucker

Dean of the Graduate College

TABLE OF CONTENTS

Chapter Page

I. INTRODUCTION 1

II. REVIEW OF LITERATURE..4

2.1. MEMS Resonators 5
2.1.1. Thermally-Transduced MEMS Resonators 8
2.1.2. Capacitively-Transduced MEMS Resonators..10
2.1.3 Piezoelectrically-Transduced MEMS Resonators 12
2.1.3.1 TPoS Resonators 16
2.2. Resonator Lumped Circuit Electrical Modeling 18
2.3. MEMS Oscillators 20
2.3.1 Capacitively-Transduced MEMS Oscillators 22
2.3.2 Piezoelectrically-Transduced MEMS Oscillators....................................23
2.4. Oscillator Topologies for Piezoelectric MEMS Devices 25
2.4.1. Trans-resistance Oscillator...25
2.4.2. Pierce Oscillator 27
2.4.3. Colpitts Oscillator 29

III. TPoS Lumped Element Circuit Characterization 32

3.1. Methodology 33
3.1.1. Scattering-parameter Fundamentals...33
3.1.2. Scattering-parameter Data Collection...34

3.2. One-port TPoS Equivalent Circuit Model 35
3.2.1 Results for One-port Parameter Extraction...37
3.3. Two-port TPoS Equivalent Circuit Model...39
3.3.1. Results for Two-port Parameter Extraction 42
3.4. Effects of Device Geometry on Device Characteristics 44
3.4.1. Perforated and Continuous Electrode Devices 44
3.4.2. Perforated Electrode with Different Hole Dimension 49
3.4.3. Substrate Thickness Effect on Resonator Behavior.................................52

IV. TPoS Oscillators...56
4.1. TPoS-Colpitts Oscillator...56
4.2. TPoS Resonator Equivalence Model for Colpitts Oscillator..........................57
4.3. Colpitts Oscillator Simulation 58
4.4. Colpitts Circuit Implementation 61

V. CONCLUSION..65

REFERENCES 67

LIST OF TABLES

Page

Table 3.1: One-port calculated equivalent model for the device under test 39

Table 3.2: Two-port finalized equivalent electrical model for TPoS 42

Table 3.3: TPoS equivalent electrical model for different center frequency devices ..43

Table 3.4: Device surface dimension in order to confirm the devices are identical in their own group (for same resonance frequency) 45

Table 3.5: Dimensions for identical devices with different hole areas 50

Table 4.1: One-port BVD elements of TPoS for colpitts oscillator implementation...57

Table 4.2: Two-port BVD elements of TPoS for colpitts oscillator implementation ..57

Table 4.3: Oscillator jitter improvement with increased voltage.................................64

LIST OF FIGURES

Page

Figure 2.1: Frequency reference circuit block diagram 5

Figure 2.2: Extensional and flexure mode for resonant structure 6

Figure 2.3: Frequency response of resonators with different quality factor 7

Figure 2.4: Thermally-transduced MEMS resonator fundamental flow diagram..........8

Figure 2.5: Two dimensional schematic view of thermally actuated I^2-BAR 9

Figure 2.6: A capacitive beam resonator device schematic 10

Figure 2.7: Fundamental schematic of piezoelectric resonators 13

Figure 2.8: Schematic of a) Thickness field excitation (TFE) b) Lateral field excitation (LFE)..14

Figure 2.9: TPoS Resonator schematic and SEM picture 16

Figure 2.10: Electrical equivalent parameters of mass-damper-spring system 18

Figure 2.11: Resonator equivalent electrical circuit a) Mason model b) Butterworth-Van Dyke model..19

Figure 2.12: Piezoelectric resonator one-port and two-port configuration.................20

Figure 2.13: Fundamental oscillator loop gain and phase condition 21

Figure 2.14: Fundamental schematic of trans-resistance oscillator 26

Figure 2.15: Conventional Pierce oscillator model...28

Figure 2.16: Conventional Colpitts oscillator model 29

Figure 3.1: Measurement set-up for S-parameter data collection...............................34

Figure 3.2: a) DUT and probe source-ground notation. b) Two-port measurement configuration...35

Figure 3.3: a) One-port device testing configuration b) Equivalent circuit diagram...35

Figure 3.4: One-port device stack dimensions and frequency response.....................37

Figure 3.5: Device motional impedance magnitude and phase response 38

Figure 3.6: a) S-parameter simulation diagram with calculated parameters b) S-parameter simulation diagram with the extracted s1p file from network analyzer......................38

Figure 3.7: Reflection parameter curve fit with finalized BVD circuit model...........39

Figure 3.8: a) Two-port device testing configuration b) Testing configuration equivalent circuit diagram 40

Figure 3.9: a) Testing configuration equivalence circuit diagram b) Simplified equivalent circuit at resonance frequency in order to derive motional resistance........................40

Figure 3.10: Two-port equivalent lumped circuit model...41

Figure 3.11: Two-port device stack dimensions and frequency response 42

Figure 3.12: Two-port finalized BVD circuit model after curve fit 43

Figure 3.13: a) Identical devices for 27MHz with continuous electrode (01) and perforated electrode (06). b) Identical devices for 54MHz with continuous electrode (27) and perforated electrode (26). 45

Figure 3.14: Resonance frequency behavior of continuous and perforated electrode for 27 MHz TPoS 46

Figure 3.15: Resonance frequency behavior of continuous and perforated electrode for 54 MHz TPoS 46

Figure 3.16: Insertion loss behavior of continuous and perforated electrode for 27 MHz and 54 MHz TPoS..47
Figure 3.17: Quality factor behavior of continuous and perforated electrode for 27 MHz and 54 MHz TPoS..47
Figure 3.18: Motional resistance behavior of continuous and perforated electrodes for 27 MHz and 54 MHz TPoS resonators 48
Figure 3.19: Motional capacitance behavior of continuous and perforated electrodes for 27 MHz and 54 MHz TPoS resonators 48
Figure 3.20: Motional inductor behavior of continuous and perforated electrodes for 27 MHz and 54 MHz TPoS resonators 49
Figure 3.21: Identical devices under test with different hole dimensions 49
Figure 3.22: Frequency shift in perforated design for different hole area 50
Figure 3.23: Insertion loss behavior in perforated design for different hole area........50
Figure 3.24: Quality factor behavior in perforated design for different hole area.......51
Figure 3.25: Motional resistor behavior in perforated design for different hole area..51
Figure 3.26: Motional inductor behavior in perforated design for different hole area 52
Figure 3.27: Motional capacitance behavior in perforated design for different hole area 52
Figure 3.28: TPoS resonator multilayer schematic..53
Figure 3.29: The change in resonance frequency in terms of substrate thickness in TPoS resonators 53
Figure 3.30: The change in insertion loss in terms of substrate thickness in TPoS resonators 54

Figure 3.31: The change in quality factor in terms of substrate thickness in TPoS resonators 54

Figure 4.1: Frequency response and device schematic of the TPoS used in colpitts implementation 57

Figure 4.2: TPoS colpitts oscillator simulation model..........58

Figure 4.3: Colpitts oscillator output 60

Figure 4.4: Colpitts implemented PC Board schematic..........61

Figure 4.5: TPoS-Colpitts Oscillator jitter measurement 63

Figure 4.6: Crystal-Colpitts Oscillator jitter measurement..........63

CHAPTER I

INTRODUCTION

Micro-Electro-Mechanical Systems (MEMS) are integrated devices which assemble electrical and mechanical systems into a compact micro-design. MEMS devices have become indispensible for the current electronic market. MEMS can refer either to a component or a system and they serve to a broad range of application areas and disciplines.

The number of components per chip has increased and due to the latest developments in IC technology and according to Moore's law these increases will continue to double every 18 months. Intel recently proposed their 22nm 3D transistor technology (Tri-gate-2011) which supports Moore's theory [1, 2]. Therefore, the small dimensions and the performance of MEMS attracts investor attention in order to develop compact, advanced and integrated circuit solutions. In Isuppli Corporation 2010 market research, a % 22 increase in demand was reported for MEMS. In the same report, the investment for MEMS applications in 2010 was reported to be approximately $8 billion. Batch fabrication of these devices enables cost efficiency. The MEMS is a promising field to replace discrete frequency selective components.

Oscillators, resonators and clocks are frequency selective devices that generate a desired reference signal for the systems [3, 4]. Electronic systems require at least one reference signal to enable system synchronization. The reference signals are defined by characteristics such as target signal frequency, frequency stability and bandwidth. All of these characteristics are set to standard values for different fields of applications. Frequency stability of an RF transceiver reference signal is required to be better than 2.5ppm where it is approximately 1ppm for GPS applications [5]. Mechanically vibrating devices (ceramics, quartz crystals etc.) have been used in reference frequency applications. Quartz crystals are unique devices by virtue of their high quality factor (Q) and high frequency stability especially for applications where high accuracy is required. Accurate and stable electronics have been manufactured with these devices. However, their relatively large package conflicts with latest technology requirements where multiple resonators may be required. Prevalent portable applications and small size electronics lead to micro-size on-chip adaptable components.

MEMS frequency selective devices offer alternative solutions for mechanically vibrating devices. MEMS are suitable for vibration applications by their rugged structure. In the recent decade, significant demand for MEMS frequency clock generators has been growing in RF applications, especially in wireless and communication systems. Research has been conducted by many groups and some commercial products have been introduced by companies in the timing industry such as Discera (MRO-100, in 2003) and Bosch (SiT8002) [5]. Meanwhile, noteworthy progress in MEMS frequency selective devices has been achieved. Today, MEMS resonators, oscillators and filters are capable of covering a wide frequency range from few kHz up to several GHz which is simply

known as radio frequency (RF) operation band. Additionally, established high selectivity, good stability, on chip integration and promising linear characteristics promotes further incentives for investments in this technology. Their low power consumption makes them appropriate candidates for portable applications, where battery life plays important role.

The objective of this thesis is to investigate the electrical characteristics of Thin-film on Substrate (TPoS) resonators and to design oscillator circuits with TPoS resonators. TPoS resonators are Micro-electro-mechanical devices (MEMS) which are coupled by piezoelectric transduction. These devices are fabricated by bulk micromachining (BAW) techniques. They present low motional impedance (few hundred Ω), and good frequency stability.

This thesis consists of five chapters. Chapter 1 presents a general introduction to MEMS frequency selective devices. Chapter 2 covers background and a review of literature. The fundamental concepts will be explained in order to provide better understanding of the methodology chapters. Also, current progress and specific studies will be reviewed to give a concrete example of the concepts that have been discussed. In chapter 3, TPoS equivalent electrical circuit modeling will be introduced. Different TPoS structures' will be modeled electronically and will be compared in order to understand the effect of certain features in each structure. In chapter 4, a TPoS colpitts oscillator circuit will be described. Simulation and PC Board implementation will be presented. Circuit behavior and important findings will be discussed. Finally, in chapter 5, the study results will be summarized. The conclusion section will relate the results of this specific study to the general concepts by emphasizing the observations.

CHAPTER II

REVIEW OF LITERATURE

In the present times, the most competitive market for resonators and oscillators is communication systems. At high RF frequencies, meeting the standards of technology becomes challenging considering the related costs, material limitations and fabrication limitations. For instance, it is stated that the frequency stability of ±0.5ppm or less is required for accurate synthesizing in prevalent GSM handsets [6]. Furthermore, high selectivity, down to % 0.1 bandwidth is required for the RF channel-selecting transceiver front-ends [7]. The frequency spectrum gets crowded by newer technologies, so the operation frequency is moved to higher levels and the percent selectivity is decreased for the carrier frequency. It is accepted that HF, VHF and UHF operations can only be achieved by scaling down the dimensions [8]. A block diagram is presented to show a cell phone frequency reference circuit in Fig. 1(a). The resonators and the oscillators are essential component in analog frequency multiplier (AFM) or in a transceiver used for front-ends, where MEMS technology is proposed to be used [9-11]. A dual mode GSM commercial product is shown in Fig. 1(b). The marked circles in Fig. 1(b) indicate the frequency selective components in a typical dual band GSM Handset [5]. It is worth mentioning that just one GSM product requires several frequency selective devices

which highlights the need and importance of this technology.

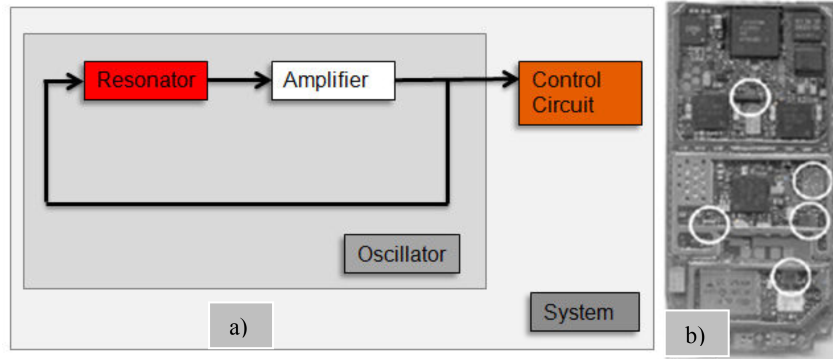

Figure 2.1: Frequency reference circuit block diagram

The focus of this study is the electrical characteristics of resonator device and its application in an oscillator circuit. In following parts of this chapter, the fundamental concepts will be introduced first and then latest reported studies will be reviewed in order to give a complete understanding of current technology. Additionally, the importance of piezoelectric devices will be emphasized in frequency selective applications.

2.1. MEMS Resonators

A resonator is a device which vibrates at particular frequencies. The frequency which the device is specifically designed for is known as fundamental frequency. The peaks at harmonic multiples of the fundamental frequency are called harmonic frequencies. Another commonly used term related to frequency response is that the spurious frequencies which are the unwanted vibrations that appear in the response. Vibration in MEMS resonators is excited by electro-mechanical energy conversion [12]. The applied electrical signal is converted to mechanical vibrations in the device and the resonant device expands, flexes or twists structurally. Fig. 2 shows the structural deformation of the resonator for different vibration modes which is simulated in COMSOL software.

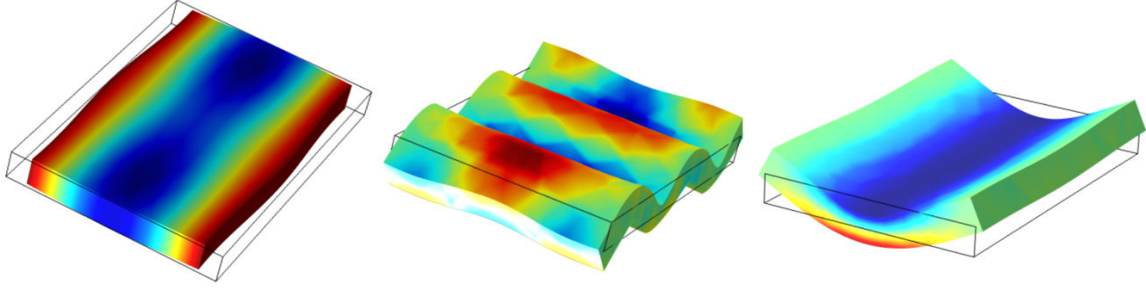

Figure 2.2 : Extensional and flexure mode for resonant structure

Resonant behavior of MEMS devices can be described by utilizing the mechanical damped harmonic oscillator equation, which is simply known as mass-damper-spring system. The mechanical damped harmonic oscillator expression is given in Eq. 2.1. The expression for resonance frequency (f_r) is derived by Eigen frequency calculation under zero applied force [12] and presented in Eq. 2.2;

$$F_o \sin(2\pi f t) = m_{eff}\frac{\mathrm{d}^2\mathrm{x}}{\mathrm{dt}^2} + \mathrm{D}\frac{\mathrm{dx}}{\mathrm{dt}} + \mathrm{k}\frac{\mathrm{dx}}{\mathrm{dt}} \tag{2.1}$$

$$f_r = \frac{1}{2\pi}\sqrt{\frac{k}{m_{eff}}} \tag{2.2}$$

$$D = \frac{2\pi f_r m_{eff}}{Q} \tag{2.3}$$

where m_{eff} is the effective mass, k is the stiffness and D is the mechanical damping. Resonance frequency is defined by stiffness and effective mass. Effective mass distribution would be different based on the device profile such as beam, ring or rectangular. Also, the stiffness is a function of Young's modulus which is an elastic material characteristic. Therefore, it can be concluded that the resonance frequency is a function of device geometry and the material properties.

Quality factor in resonators is defined as a measure of stored energy over dissipated energy. As it is given in Eq. 2.4 the quality factor is inversely proportional to 3dB bandwidth B. Thus, high Q would stimulate sharp amplitude increase in frequency response. Narrow bandwidth improves the device frequency selectivity. Hence, relatively high Q resonator is necessary for high selectivity operations. For instance, RF channel-selecting transceiver front-ends which require approximately % 0.1 selectivity [7].

$$Q = \frac{Energy\ transfered}{Energy\ dissipated} = \frac{f_r}{B} \tag{2.4}$$

In literature, the product of resonance frequency and the quality factor (f_rxQ) is commonly used when addressing the efficiency of resonators. These parameters can be measured directly with a network analyzer. Measurement details will be explained in the chapter 3. The frequency response of the two resonators with different Q is presented in Fig. 3. From figures it can be seen that high Q device present a clean sharp frequency response.

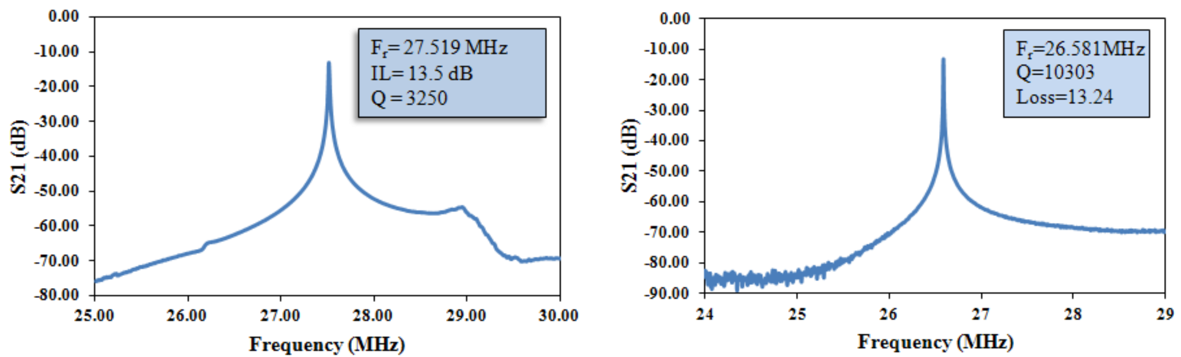

Figure 2.3 : Frequency response of resonators with different quality factor

At the present, RF MEMS resonators are capable of achieving very high f-Q product (approximately 2.75×10^{13}) and good temperature stability (≤18ppm) within very small

(few-µm) dimensions [9, 13]. Although the need for crystal-based frequency selective devices still continues, on-chip integration of MEMS structures provides a big advantage compared to quartz crystals.

A variety of electro-mechanical energy conversion mechanisms have been studied for MEMS devices. Electrostatic, piezoelectric and thermal actuators are more common transduction types compare to other mechanisms (electromagnetic) due to their simple design structure and higher efficiency.

2.1.1. Thermally-Transduced MEMS Resonators

Thermal actuation is a well-known mechanism that has been used for sensor applications for many years. Thermally actuated resonant devices are proposed as strong candidate for next-generation, highly integrated nano-mechanical applications. These devices perform better in nano-scale as opposed to capacitive and piezoelectric devices. Simple design structure, low operating voltage and large actuation force are some advantages of thermally actuated systems [14]. The thermally-transduced resonator working principle is divided into subsystems and shown with a flow diagram in Fig. 4.

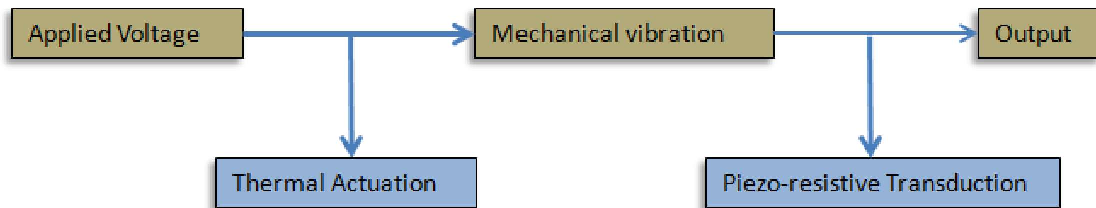

Figure 2.4: Thermally-transduced MEMS resonator fundamental flow diagram

Thermal resonators require both AC and DC sources. The applied DC voltage to the device input would cause resistive heating in extensional pillars. The heating leads

thermal fluctuations and material expansion occurs. Material expansion changes the resistivity in pillars which would modulate the input DC current and generates an AC output. AC output current is named as motional current [14, 15]. The mechanical vibration frequency equates to input AC signal frequency at certain point. This point is the frequency where the resonator operates in its in-plane extensional mode.

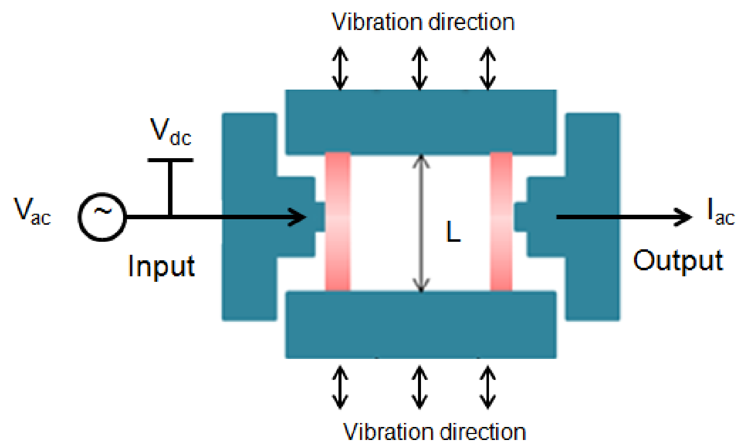

Figure 2.5: Two dimensional schematic view of Thermally actuated I^2-BAR [14]

Low output resistance is an advantage for the IC integration of devices. Thermally actuated resonators present very low output resistance that few tens of Ωs and even less than 10Ω are reported [14]. On the other hand, the reported f-Q products for thermal devices are slightly under the average of MEMS resonator results reported in literature up to date. In [15] different dimensions have been studied and the best f-Q product is reported to be approximately $1.5x10^{12}$ for one specific design. Despite all the advantages, thermally actuated devices dissipate large amount of power. Since the main principle is based on resistive heating, these devices are exposed to high body temperature which might limit the operation. Although thermally-transduced devices are stated as slow due

to the required time to reach up to desired heat level, advance designs can overcome this problem [14].

2.1.2. Capacitively-Transduced MEMS Resonators

Due to very high quality factor, capacitive devices attract many researchers' attention and substantial amount of research has been conducted in the area of capacitively-transduced MEMS resonators.

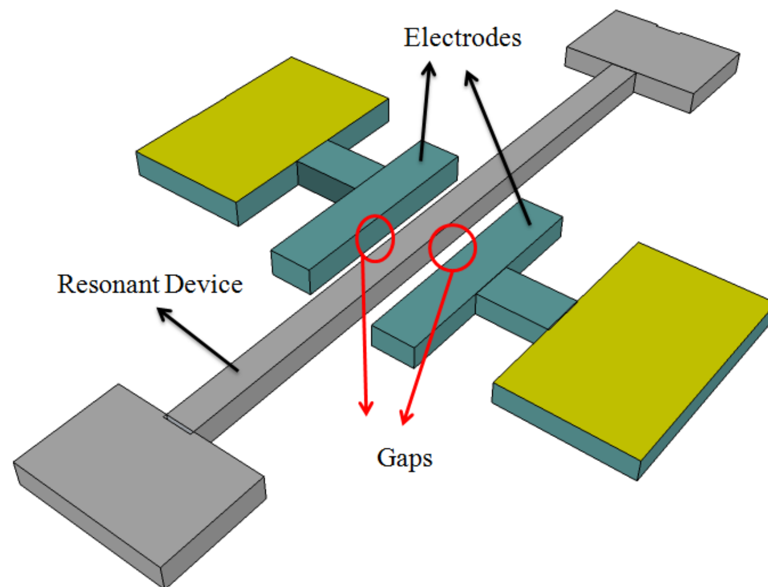

Figure 2.6 : A capacitive beam resonator device schematic [16]

A simple schematic of one type of beam electrostatic resonator is given in Fig. 6. An applied DC polarization voltage creates an electric field between the electrodes which excites the device vibration. Capacitively-transduced resonators are also named as electrostatic resonators as well. There is variety of capacitively-transduced design established. Disk resonators, ring resonators, Free Free-Beam, Clamp Clamp-Beam and vertical silicon bulk acoustic resonator (SiBAR) are commonly known electrostatic designs which are different from each other geometrically. Disk and ring geometry are

two popular capacitive architectures which exhibit remarkable performance results. Radial contour mode disk resonator has been reported to have the highest series resonant Q published (~71400) for 299.86MHz [17]. In this study, the loss is decreased by acoustic mismatch. Also the introduced deposition technique in this study enables poly-diamond deposition for much lower costs [17]. Another radial-contour mode poly-silicon disk resonator has been studied by W. Jing et al., and Q≥1500 for 1.14GHz is measured in both air and vacuum achieving Q~7330 in vacuum and Q~6100 in air at 733MHz resonance frequency [18]. W. Jing et al. has enhanced corresponding design with creating acoustic mismatch by placing poly-silicon between the nano-crystalline diamond disk and the stem [9]. The acoustic mismatch minimizes the energy dissipation between disk and stem. Thus, decreased anchor loss leads as such high quality factor.

Motional impedance in electrostatic devices is a strong function of gap size. Capacitive devices suffer from high motional impedance, in the range of several kΩs [7-9]. High motional impedance complicates the integrated circuit topology that would lead to additional gain stages and control circuits. Extra gain stages, PLL controllers and additional transistors may increase the circuit noise floor. The methods for reducing the motional impedance of electrostatic devices have been reviewed in [19] and encouraging low impedance (few-hundreds) results have been reported [19-21]. Fabricating resonators with very small gap size is the conventional approach in order to reduce device motional impedance. Also, increasing actuation area has been proposed as another approach. But both approaches are limited by fabrication technology. A recent idea of placing dielectric material in the gap is studied. In 2004, Sheng-Shian Li, et al. has demonstrated poly-silicon “hollow disk” ring resonator structure which exhibit 282 kΩ motional impedance

[7]. Furthermore, vertical capacitive SiBAR design has been proposed as low motional impedance (few kΩs) by S.Pourkamali et al. [20]. Array-disk resonator design presents the most encouraging results for low motional impedance with very high quality factor. However, the array configuration would increase the dimension of chip which makes their IC integration challenging. Also, fabrication tolerances cause mismatches in capacitive devices where trimming becomes crucial for array designs [8].

Beam resonators have shown good low frequency performance. However, they require excessive scaling down (to nano-dimensions) to enable several MHz and GHz frequencies which brings some practical limitations to usability of beam-devices [13]. For instance, nano-scale devices are capable of handling less power than what is required today at technology which would complicate the circuit topology. In addition to this, nano-scaling can induce circuit noise which is caused by temperature fluctuations [8, 13]. Despite all the impressive Q and f-Q product results, electrostatic devices have not become successful for high volume products in communication field.

2.1.3. Piezoelectrically-Transduced MEMS Resonators

Piezoelectric devices have shown success as a high volume product due to their ease in fabrication and remarkably low motional resistance (tens of Ω's) [22, 23]. Low motional resistance of these devices gives opportunity to work with single transistor circuits where the circuit phase noise and selectivity improves significantly.

Piezoelectricity was discovered in 1880 by the Curie brothers. In 1881, Lippmann proposed bidirectional property of piezoelectricity by using thermodynamic theory on direct piezoelectric phenomenon. In the direct piezoelectric effect, electric charge is

generated by applying an external force to the material. On the other hand, in converse piezoelectric effect, material shows mechanical strain as a result of applied electric field [24].

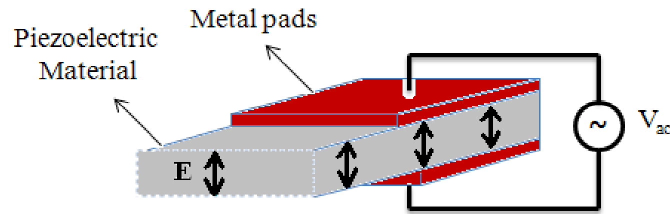

Figure 2.7: Fundamental schematic of piezoelectric resonators

In order to understand the stress, strain and electric field relation, the electrical and mechanical behavior of piezoelectric materials are simply expressed with a couple of fundamental equations:

$$D = \varepsilon^T \mathrm{E} + \mathrm{dT} \quad (2.5)$$

$$S = \mathrm{d_t E} + \mathrm{s^E T} \quad (2.6)$$

where, D represents the electrical displacement, T is the stress, E is the electric field, s^E is the compliance under constant electric field. Also, the permittivity at constant stress is given as ε^T and the piezoelectric constant is given as d.

Piezoelectricity relates the electrical behavior and the elastic behavior of the dielectric materials [24]. Applied alternating voltage builds an electric field in material which causes polarization. Eq. 2.5 shows the relation between electrical field and stress. Strain, which is the mechanical displacement, occurs as a result of applied electric field, is given in Eq. 2.6.

Two main classes of the piezoelectric MEMS resonators are categorized as surface acoustic wave (SAW) and bulk acoustic Wave (BAW). The acoustic wave propagation takes place along the surface in SAW devices; on the other hand the acoustic wave travels through the bulk in BAW devices. SAW resonators are large in size and incompatible for microelectronic integration [25]. BAW resonators are favored by their high f-Q product, low insertion loss and high power handling [26]. Thickness field excitation (TFE) and lateral field excitation (LFE) are commonly known implementations that have been studied and their principle is presented in Fig. 8.

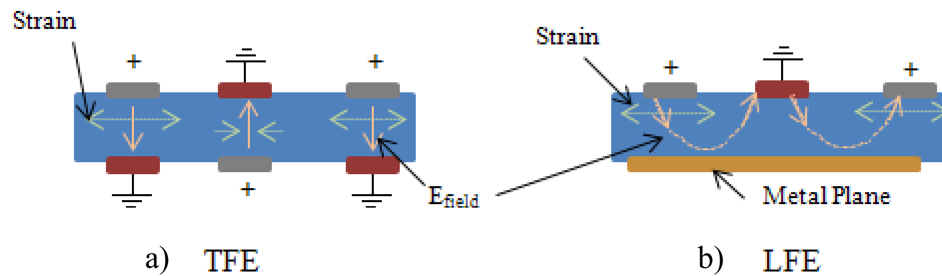

Figure 2.8: Schematic of a) Thickness field excitation (TFE) b) Lateral field excitation (LFE) [22]

BAW devices consist of multilayer. The piezoelectric material is sandwiched between metal electrodes. The device is excited by the applied alternating voltage. The piezoelectric material contracts or expands as a function of applied voltage. It can be observed from the Fig. 8 that the vibration configuration is defined by the electrode pattern [27]. But also the material crystalline properties play a role to define mode of vibration [24]. Thin film bulk acoustic resonator (FBAR) is a well-known BAW device and usually they are designed based on TFE. Lateral extensional devices come over frequency shift problem by their robust structure and their less sensitivity on electrode patterning. Lateral mode of vibration can be excited by enabling d_{31} transverse

piezoelectric coefficient where strain in TFE is related to d_{33}. Piezoelectric "d" coefficient basically relates amount of strain over the applied electric field. Both TFE and LFE piezoelectric devices have been proposed as attractive candidates for communication systems.

Piezoelectric devices present high electromechanical coupling coefficients (≥2 %) [22, 28]. The highest f-Q product for piezoelectric resonators is reported as $\sim 10^{14}$ by P. Wei et al., in [26]. This study utilizes Aluminum nitride (AlN) piezoelectric material on a sapphire substrate. Recently G. Songbin et al. demonstrates 0.75×10^{13} f-Q product for AlN material on Silicon Carbide (SiC) substrate [29]. In both study, this high of an f-Q product is also influenced by substrate material properties of sapphire and SiC. However, silicon keeps its popularity as most favored substrate because of the cost and ease manufacturing.

In order to investigate silicon substrate thickness effect on Q and power handling, AlN on silicon substrate resonators are used [30]. Two different substrate thicknesses, 30μm and 20μm Silicon, are investigated. The improvement in Q by the factor of 2.5 is reported for 34 % increased thickness and f-Q product is reported as 0.7×10^{13} for 1 GHz [30]. The resonance frequency is a function of device width in lateral mode resonators. The resonator fundamental frequency increases by reducing the device width. Achieving UHF fundamental mode operation requires advance designs and very small dimensions. The fabrication tolerances become more effective for the devices with very small dimensions (few microns). Multi-electrode design is one approach which reduces the dependency of frequency response to lithographic limitations [22]. Moreover, B. P. Harrington et al., showed in their study that multi-tether approach for the thin film

piezoelectric on substrate (TPoS) resonators suppresses undesired modes by removing near-resonance distortions [31].

In the next section, TPoS resonator is introduced which is the core device of the oscillator circuit that has been performed in this study. TPoS is a piezoelectric resonator which vibrates in lateral mode and is listed in the class of BAW devices.

2.1.3.1.Thin film Piezoelectric on Substrate (TPoS) Resonators

TPoS resonators consist of a piezoelectric material which is sandwiched between two metal electrodes. In TPoS resonators the device is mounted on a substrate and the resonant device vibrates in lateral mode. TPoS resonators are in the category of BAW devices in which the acoustic wave propagates through the bulk. Thus, the substrate, which is made up of a high energy density material, would decrease the acoustic loss. Improved quality factor is shown with a low acoustic loss substrate. It is reported in [30] that the thickness has enormous effect on frequency response. The fundamental schematic for TPoS device is given in Fig. 9. The silicon is used in this device as the substrate material. SEM picture a TPoS design is also given in Fig. 9.

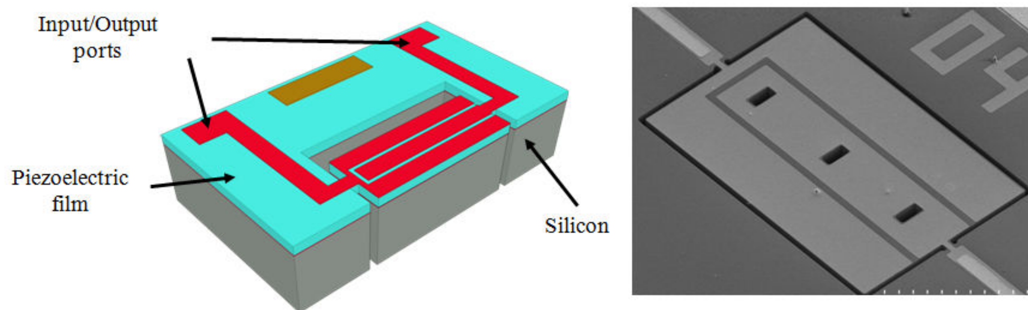

Figure 2.9. TPoS Resonator schematic and SEM picture

The overall quality factor in TPoS resonators is a function of several variables and the expression is given in Eq. 2.7.

$$Q = \left(\frac{1}{Q_{material}} + \frac{1}{Q_{anchor}} + \frac{1}{Q_{air}}\right)^{-1} \tag{2.7}$$

Air damping is the least effective factor for the frequencies which are larger than a few MHz in TPoS resonators. The TPoS shows very close frequency characteristics in air and under vacuum in those frequencies. This behavior of TPoS is very favorable because it simplifies the packaging step. The anchor loss can be reduced by building In-plane acoustic reflectors approach that shows 560 % Q enhancement and it is reported in [32]. Finally, the material damping is the dominant factor which is known as irreversible loss mechanism. It also indirectly limits the maximum quality factor of the device [33].

$$E_{max} = \frac{1}{2} k_0 x_c^2 \tag{2.8}$$

$$k = \frac{n^2 \pi^2 A\, E}{2L} \tag{2.9}$$

E_{max} is the maximum power that the device can handle. k_0 and x_c are stiffness and vibration amplitude respectively. Power handling of TPoS is limited by nonlinearities and nonlinearities are related to the stiffness. In Eq. 2.8, the linear system has been defined with only one spring constant. However, in nonlinear case there will be nonlinear spring constants which amplify the harmonic vibration amplitude in resonator. The frequency shifts would occur and the largest power that device can handle reduces. It is clear from Eq. 2.9 that the stiffness is proportional to device thickness. The nonlinearity improves with large thickness and it is demonstrated in [30].

Superior low motional resistance characteristic in the range of few hundred Ω's make TPoS a very attractive candidate for oscillator and filter applications. TPoS resonators can be used either one port or two port. Port configuration is decided based on the application and the device electrical characteristics would be different according to port configuration. The port configuration will be introduced in the following section. The detailed information for one-two port configuration is given in chapter 3.

2.2 Resonator Lumped Electrical Modeling

Resonator behavior can be modeled either with analytical expressions or electrical equivalent circuits. Mechanical behavior of resonators can be expressed by electrical parameters and the device can be simplified to an RLC circuit. A simple RLC circuit model gives clear insight into resonator characteristics. Also it provides opportunity to integrate relevant MEMS device into CAD simulation tools. Thus, detailed circuit analysis can be done with simulation software before device circuit implementations. Fundamental mass-damper-spring system expression and its equivalent electrical circuit are given in Fig. 2.10.

$$V(t) = L\frac{\mathrm{di}}{\mathrm{dt}} + \mathrm{Ri} + \frac{1}{\mathrm{C}}\int \mathrm{idt} \qquad (2.10)$$

$$\mathrm{R} = \mathrm{D}, \qquad \mathrm{L} = m_{eff}, \qquad \mathrm{C} = \frac{1}{\mathrm{k}};$$

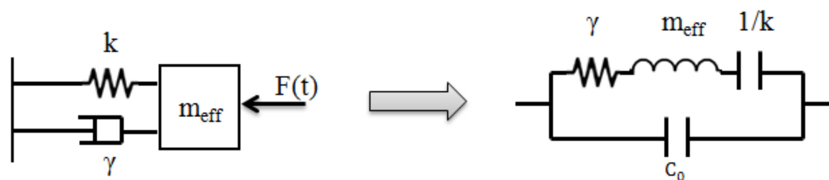

Figure 2.10: Electrical equivalent parameters of mass-damper-spring system

Resonance frequency of the RLC circuit is given in Eq. 11.The quality factor of the equivalent circuit is also expressed in Eq. 2.12.

$$f_r = \frac{1}{2\pi\sqrt{LC}} \tag{2.11}$$

$$Q = \frac{1}{2\pi RC} = \frac{2\pi f_r L}{R} \tag{2.12}$$

Electrical resistor (R) represents mechanical damping (D); the inductor and the capacitor are parameters associated with the effective mass and the stiffness respectively. Resonators can be characterized by Mason transmission line model but for oscillator integration purposes Butterworth-Van Dyke (BVD) is more convenient approach due to its simplicity [34]. Both circuit models are given in figure 11.

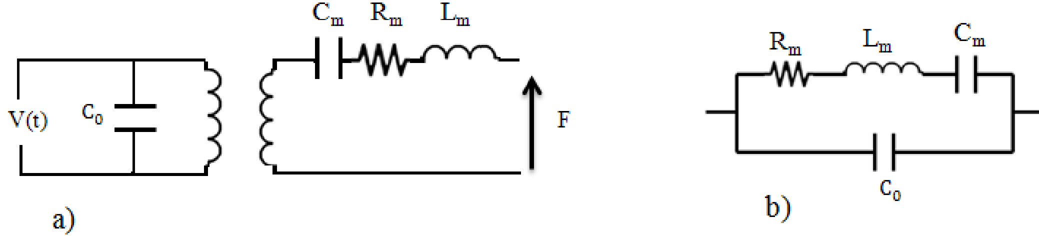

Figure 2.11: Resonator equivalent electrical circuit a) Mason model b)Butterworth-Van Dyke model

R_m, L_m and C_m are the elements of the motional arm. Also the element C_o represents the intrinsic capacitance which is present between the input and output terminal. The motional arm equivalence is already presented above. In addition to this the parasitic capacitance expression, C_o, is given as:

$$C_o = \varepsilon_p \frac{Electroded\ Area}{Electrode\ Thickness} \tag{2.13}$$

According to the resonator geometry, different parameters would dominate in device characteristics. Therefore, modified BVD models exist for specific studies although the core circuit stays the same. Resonant devices can be categorized as one-port and two-port regarding to their input-output configuration. In one-port, input and output is taken from the two opposing electrodes on the piezoelectric film. On the other hand, in two-port, the input and output are isolated from each other.

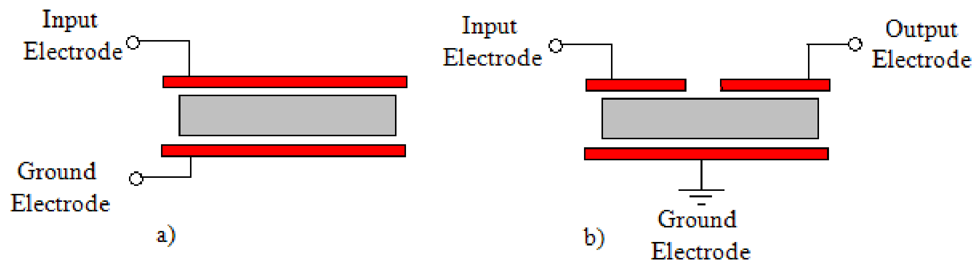

Figure 2.12: Piezoelectric resonator one-port and two-port configuration

The most noticeable advantage of two-port design is the electrical isolation of input and output ports [35]. This configuration is quite suitable for transformer applications. Also two-port configuration present very low intrinsic capacitance compare to one-port.

2.3 MEMS Oscillators

Oscillator is a positive feedback loop which consists of an amplifier and a frequency selective component. Mechanical resonators are integrated in oscillator circuits in order to generate required clock signal. Linear electronic stability conditions are studied by German physicist Heinrich Georg Barkhausen who has determined the essential gain and phase conditions for oscillation which is known today as Barkhausen criterion in literature. Oscillation in a circuit would start only if the Barkhausen criterions

are satisfied. The Barkhausen conditions state that the feedback loop gain should be equal or greater than 1. In addition to this, the phase shift around the feedback loop should be zero or multiples of 360°.

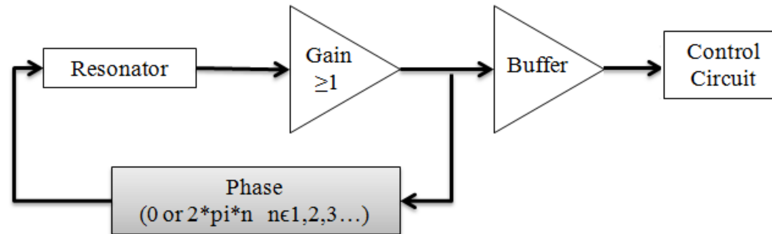

Figure 2.13: Fundamental oscillator loop gain and phase condition

MEMS oscillators are demanded due to their shorter lead times, small sizes and low cost. MEMS offer more configurability to customize the device to specific applications. Multiple frequency applications can be achieved by electronic control circuits using just one resonator. Significant low phase noise (-165dBc/Hz at 1 MHz offset) and high temperature stability (-2.4ppm/°C) results are reported [11, 36].

There are several attributes that should be taken into account in order to achieve a successful MEMS oscillator design such as quality factor, stability, nonlinearity and geometric flexibility [13]. Oscillator output frequency is determined by the frequency reference tank circuit. It is clear that the overall oscillator performance is dependent on the resonant device but also it is dependent on the oscillation sustaining circuit topology as well. Appropriate circuit topology would vary due to the resonator device properties and the application purposes. For instance, relatively complicated circuits are necessary for capacitively-transduced devices because it is more challenging to satisfy oscillation start-up conditions according to their high motional impedance. On the other hand,

piezoelectrically-transduced resonator devices succeed to operate with very simple circuit configurations even with a single transistor. In the following parts, electrostatic and piezoelectric oscillators will be reviewed. Then, trans-resistance, pierce and colpitts circuit topologies will be introduced.

2.3.1. Capacitive MEMS Oscillators

Electrostatic MEMS oscillators are proposed as promising candidate for communications systems. Low phase noise and low power consumption of electrostatic based MEMS oscillators attract the research interest. Even though the batch manufacturing is not achieved yet; encouraging results have been reported in literature.

Phase noise (frequency domain) or jitter (time domain) is an important characteristic for the understanding of overall oscillator performance. It is desired to have a low phase noise oscillator to avoid unwanted frequency distortions. Since the oscillator phase noise is inversely proportional to the resonator quality factor, high quality factor resonators are desired for oscillator applications [37]. As it was discussed in section 2.1.2, the electrostatic resonators present very high quality factor in the order of tens of thousands at high MHz frequencies and GHz frequencies. A wine-glass-mode disk resonator array oscillator is studied by L. Yu-Wei et al., and the phase noise is reported as -123dBc/Hz at 1 kHz offset for 60MHz center frequency [38]. In this study, the disk resonator array is scaled down to 10 MHz and the quality factor is noted as 48,000. The author emphasizes that the reported oscillator phase noise was higher than what was expected for such high quality factor resonator array and they have related this high phase noise result to the $1/f^3$ noise component which is caused by resonator nonlinearities.

The power levels of the oscillator effects the resonator nonlinearity. The trade-off between quality factor and power handling in resonator devices lead to optimization of resonator and sustaining circuit power level of in order to obtain good overall performance. Two different automatic level control mechanisms are explored in order to reduce noise component [39]. One is gain control of the sustaining circuit with adjusting circuit elements proposed as "gain-ALC". The other explored mechanism is the motional resistance control with variable DC-bias voltage which is introduced as "V_p-ALC". The relative circuit diagrams are given in [39] for both ALC mechanisms.

High motional resistance of the electrostatic devices (more than few kΩ's) is the biggest challenge in this technology. The approaches in order to reduce resonator motional resistance are still inadequate to satisfy market standards and the studies continue for proposing an effective solution. Simple oscillator topologies with a single transistor are impractical for electrostatic resonators since the sustaining circuit gain is insufficient to compensate high loss caused by high motional resistance. Therefore, electrostatic oscillators are more complicated in principle than piezoelectric relatives.

2.3.2. Piezoelectric MEMS Oscillators

Piezoelectric-activated oscillators have been used for frequency synthesis and they are successfully penetrated in communication electronics. In the piezoelectric oscillator, the main vibration component is the electrically excited piezoelectric film. Thin film piezoelectric resonators present low motional resistance (few tens of Ωs) and excellent power handling which enable the single stage oscillator topologies.

Piezoelectric based oscillators are commonly shown as good candidate for low phase noise, low power and high frequency oscillators.

Low phase noise oscillator results have been demonstrated. A dual-mode high-Q AlN MEMS resonator is implemented in the tunable oscillator for 1.94GHz operation frequency [40]. This study has reported the best phase noise for CMOS oscillators that has been published yet (2011) as -71dBc/Hz at 1 kHz offset with a -155dBc/Hz noise floor at 1MHz. Square extensional mode single crystal silicon resonator based MEMS oscillator is reported with a phase noise floor of -147dBc/Hz for 13 MHz center frequency [41]. The common benefits that all piezoelectric oscillators provide can be listed as the elimination of extra gain stage, automatic level control circuits (ALC) and bias voltage needs [42]. Thus, the circuit is simplified to a few components, which would lead to improve the overall oscillator phase noise.

Both oscillators that have been discussed in the above papers are designed based on pierce circuit model. Pierce and trans-resistance are commonly used oscillator topologies in piezoelectric-MEMS oscillators. The trans-resistance circuit is more preferred for relatively high motional resistor type resonators because the sufficient gain is easily provided for oscillation start-up. Trans-resistance amplifier with TPoS resonator is studied in [36] and the lowest power consumption for 106MHz resonance frequency is reported as ~350μW. This study achieves oscillation with a very simple sustaining circuit model. The oscillator far-from carrier phase noise is reported as -145dBc/Hz where the close-to-carrier phase noise is -88dBc/Hz at 1 kHz offset. Piezoelectric MEMS oscillator sustaining circuits follows the quartz implemented circuit trends according to their similar characteristics. Although colpitts is a famous quartz oscillator topology, this

circuit model has not been studied for MEMS piezoelectric oscillator according to some challenges which are discussed in detailed through chapter 4.

Temperature based frequency stability is another important aspect in addition to oscillator phase noise and quality factor. The typical temperature coefficient factor (TCF) value vary with the average of ~ (-20ppm/^{o}C) for piezoelectric devices. Favorably, quite promising techniques have been demonstrated to decrease resonator TCF down to -2.4 ppm/^{o}C [36].

2.4 Oscillator Topologies for Pieoelectric-MEMS

Different circuit configurations exist for MEMS oscillators. The understanding of the resonator tank circuit characteristics plays a key role to build an efficient oscillator circuit. Pierce circuit model is quite popular in MEMS applications due to their high frequency stability. Trans-resistor oscillators are capable of satisfying oscillation condition for a wide range of resonator type. Colpitts oscillators present low phase noise however they are more challenging to implement compared to previously mentioned two oscillator types because of the Miller capacitance effects.

The three oscillator topologies, trans-resistance, pierce and colpitts are introduced in the following sections of this chapter. Practical models are given for each and circuit principles are explained.

2.4.1. Trans-Resistance Oscillators

Shunt-shunt feedback configuration is a popular positive feedback loop for MEMS which is also known as trans-resistance oscillator. Shunt configuration at both

input and output helps reducing the input and output impedance. Trans-resistance oscillators are capable of providing relatively high gain, which increases the tendency of oscillation [43]. According to its high gain capability, this oscillator topology is compatible with high motional resistance MEMS resonators. Basic circuit model for trans-resistance oscillator is given in Fig. 14.

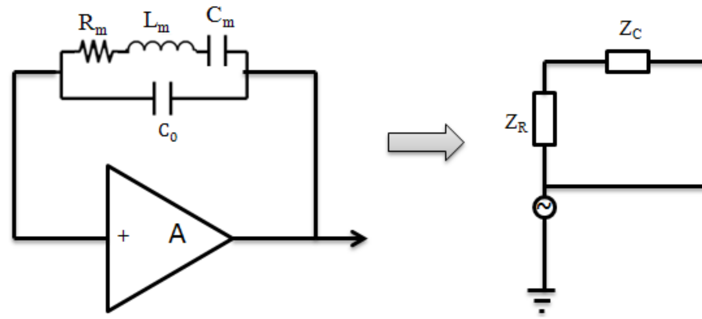

Figure 2.14: Fundamental schematic of trans-resistance oscillator

The principle model of trans-resistance circuit can be analyzed by splitting the model into two main parts, resonator and sustaining circuit [44]. Z_R is resonator impedance and Z_C is the circuit impedance.

$$Z = R(Z) + Im(Z) \tag{2.14}$$

The oscillation starts where the positive resonator impedance is equal to active circuit impedance which is expressed in Eq. 2.15.

$$Z_R = Z_C \tag{2.15}$$

Eq. 2.15 is given in literature as the amount of required negative resistance that the active circuit supposed to provide. Although there is no negative resistance exists in practice, this is a theoretic definition in order to emphasize that the resonator loss is compensated

by the active circuit. Thus, the overall gain starts amplifying. If the phase condition is satisfied simultaneously, the oscillation builds up with a time constant. The time constant which is the required time for the frequency stabilization for trans-resistance oscillator is given in [44] as:

$$\tau = -\frac{L}{R(Z_C) + R(Z_R)} = -\frac{1}{\omega^2 C[R(Z_C) + R(Z_R)]} \tag{2.16}$$

The excellent characteristics of MEMS piezoelectric resonators reduce the need for high gain. Thus the trans-resistor oscillator can be simplified to a single transistor and a few resistors [36]. After the oscillation starts, the gain can be stabilized by a feedback system or some extra control circuits which would be placed after the amplifier. The critical negative resistance point which is a function of amplifier trans-impedance value has been studied by [44] and the locus plots are presented.

Trans-resistance oscillators present fast start-up compare to Pierce and Colpitts.. Although trans-resistance oscillators have good frequency stability, the stability depends on both the resonator and the active circuit characteristics. The common drawback that has been reported in literature for trans-resistance oscillators is that they consume more power than other configurations. However, there is no complete power analysis done to make an accurate comparison in power consumption respect.

2.4.2. Pierce Oscillator

Although pierce oscillators are essential topology for quartz applications, also they have been successfully integrated with MEMS based resonators [11, 27, 41]. The negative resistance that can be supplied from the pierce is dominated by the parasitic

capacitance of the resonator device. In addition to this, the maximum negative resistance that can be obtained from pierce is lower compared to trans-resistance oscillators. Thus, this topology is more favored for MEMS piezoelectric resonators since they have relatively low motional resistance. A basic pierce model is given in Fig. 2.15.

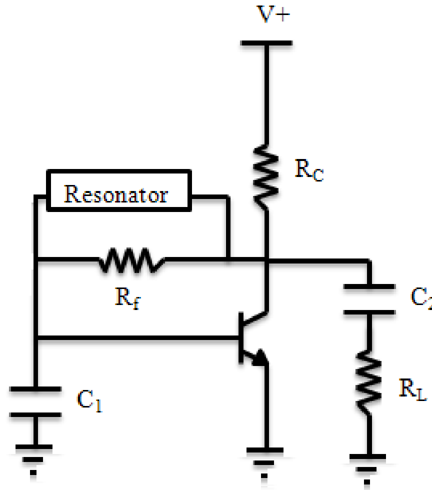

Figure 2.15: Conventional Pierce oscillator model

In the circuit diagram, R_f is negative feedback resistor that controls the collector current and improves stability [43]. The oscillator gain is given by the ratio of C_1 / C_2. The negative resistance that can be obtained from pierce is given in Fig. 2.17 [44].

$$R(Z_C)_{max} = \frac{1}{2\omega C_a(1 + \frac{C_i + C_o}{C_i C_o} C_a)} \tag{2.17}$$

C_i and C_o are input and output capacitances respectively. C_a stands for the parasitic capacitance caused by the resonator structure.

Pierce circuit is easy to implement and no DC bias voltage is required. Low phase noise (-165dBz/Hz at 785MHz) is reported as common characteristics of MOS-based pierce circuits. Integrated MOS enabled pierce circuits are studied for multi-frequency

applications [11, 27]. Pierce eliminates the need for power-hungry PLL circuits and shrinks the oscillator chip size.

2.4.3. Colpitts Oscillators

Colpitts oscillator which is invented by Edwin Colpitts is a commonly used topology in oscillator applications. Typical characteristic of Colpitts oscillator is that its capacitive feedback structure which improves short term stability and helps to decrease the phase noise. Conventional colpitts oscillator circuit model is given in Fig. 2.16.

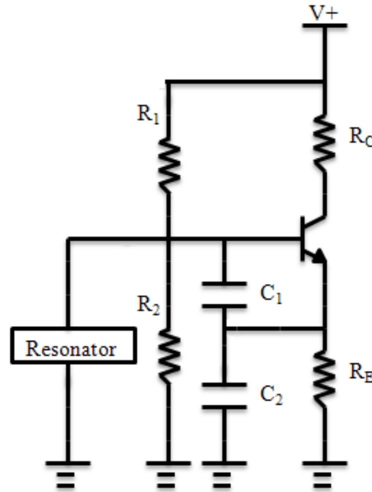

Figure 2.16: Conventional Colpitts Circuit Diagram

As it is mentioned in previous circuit topologies, gain and phase conditions should be satisfied for all oscillator circuits in order to sustain oscillation. Negative resistance value of active circuit is given as a critical criterion which is related to gain condition. Conventional colpitts negative resistance formulation has been studied in [45] and it is given as:

$$-R = -\frac{g_m}{\omega^2 C_1 C_2} \frac{2\, I_1(x)}{x\, I_0(x)} \tag{2.18}$$

In the first half of the equation; g_m is the transistor trans-conductance and the C_1, C_2 are the feedback capacitances as they are noted in Fig. 2.16. In the second portion, x represents the relative oscillation amplitude. Therefore, Eq. 2.18 shows the dependency of negative resistance to the oscillation amplitude. However, the analytical equations are not presented here in detail because it is not the main focus of this study. Only the derived negative resistance formulation is provided to give insight of circuit principle. The R_1 and R_2, which takes place in the voltage divider, and also the emitter resistance R_E are large compare to capacitor impedance [45]. Therefore, the signal passing through this network is neglected.

The colpitts oscillator is more common in quartz based applications according to quartz's very low motional resistance (few tens of Ω) [46]. The configuration in which the output is taken from collector improves the emitter loading. Thus the need for buffer stage is eliminated. However, achieving negative resistance in high frequency range with colpitts is difficult due to miller Effect [43]. The miller effect is caused by the collector and base junction parasitic capacitances [46]. At high frequencies, the large parasitic impedance reduces the negative resistance which is critical for oscillation start-up. When the negative resistance of the active circuit reduces lower than the resonator motional resistance, the circuit becomes insufficient to compensate the resonator losses. Thus, the oscillation would be damped [47, 48]. Different approaches have been studied in order to reduce miller effect and modified circuit models have been reported. A GHz frequency crystal operation is demonstrated by N. Nomura et al. and modified colpitts model is proposed with adding an emitter follower to the conventional colpitts [49]. Also, placing feedback capacitor between collector and emitter in order to reduce emitter voltage to

enable a low drive level colpitts is reported as alternative colpitts model [47]. A simple technique is proposed by Y.Chen et al. that an inductor is placed between collector and base junctions in parallel to miller capacitance [46]. Furthermore, VCO circuits are demonstrated for colpitts [48, 50]. The 454 MHz center frequency VCO colpitts for frequency tuning is reported with -122dBc/Hz at 100kHz offset [50].

In chapter 4, a modified colpitts oscillator will be implemented by utilizing a 27 MHz TPoS resonator. The circuit principle will be discussed in detailed with the simulation model and PC Board circuit.

CHAPTER III

TPoS Lumped Element Circuit Characterization

MEMS resonators can be expressed with an equivalent electrical circuit model. Knowing the equivalent electrical model of a MEMS resonator provides the opportunity to integrate device into simulation environment. Since the target of this study is designing an oscillator circuit by utilizing TPoS resonators, equivalent circuit extraction is essential and it can be noted as an early step of oscillator design process.

TPoS electrical characteristics are influenced by the device's mechanical and acoustic properties. Operation frequency, substrate thickness and device pattern are some examples of these properties which affect electrical characteristics. Different patterns such as perforated electrode and continuous electrode are designed and a variety of center frequency devices are fabricated with different substrate thickness.

This chapter consists of two main parts. First, TPoS resonator one-port and two-port electrical model extraction is demonstrated. Secondly, the effects of structural diversities on device electrical characteristics are investigated. The resonance behavior for perforated and continuous electrodes is compared between 27 MHz and 54 MHz devices. The substrate thickness effect is then studied by testing identical devices which are fabricated on 10 µm and 25 µm silicon.

3.1 Methodology

The equivalent electrical circuit of the TPoS resonator is experimentally extracted by using scattering parameters (S-parameters). Butterworth Van-Dyke Model (BVD) is used as theoretical model which has been introduced in the background section. BVD circuit elements are calculated with the collected data from the network analyzer. The calculated lumped circuit model is simulated in Advance Design Systems (ADS). In addition to this, another simulation is run for a characterized blackbox in ADS with the directly measured S-parameter data from the network analyzer. The calculated parameters are optimized by curve fitting. Thus, the finalized calculated circuit model frequency response meets the directly measured frequency response of device. These final circuit elements are reported as extracted equivalent electrical model of related TPoS resonator.

3.1.1. Scattering-parameter Fundamentals

Resonator devices are modeled by using transmission networks. The transmission networks in RF operation frequencies are characterized by various parameters. At high RF frequencies (MHz and GHz), hybrid (h) and scattering (S) parameters are commonly preferred for network characterization. Although impedance (Z) parameters seem more practical for equivalent circuit extraction, they are not preferred in the applications for high operation frequencies because the open-short circuit condition is difficult to implement at high frequencies where the complex impedance plays an important role. Low frequency (kHz's) systems are usually described by admittance (Y) and impedance (Z) parameters [51]. S-parameters are a measure of transmitted and reflected waves and

they can be determined by a network analyzer (NA). NA is an instrument which analyzes transmission line characteristics between defined frequency spans and it acquires both magnitude and phase measurements. S-parameters are used in this study to extract TPoS-resonator electrical circuit model.

3.1.2. Scattering-parameter Data Collection

S-parameter measurements are performed by an Agilent E8358A PNA series Network Analyzer. Device under test (DUT) is connected to NA with 150 μm pitch GSG ZProbes and the probes are connected to 50 Ω terminations. DUT is placed onto a SUSS-Microtech test system and measurements are taken in air, at room temperature. Picture of measurement set-up is presented in Fig.3.1.

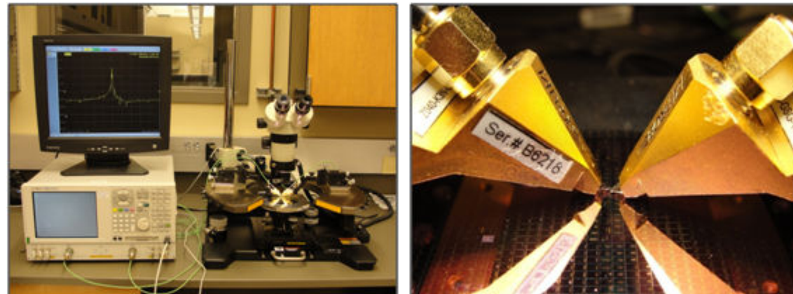

Figure3.1: Measurement set-up for S-parameter data collection

Accurate data collection requires some previous steps before testing the device. The network analyzer is calibrated in order to avoid systematic measurement errors. The calibration is performed by using SUSS CSR-8 calibration substrate. Open-short-load-through connections are applied during calibration respectively. The sweep range was centered to the desired resonance frequency. Small IF bandwidth is set to decrease random measurement errors. The number of sweep points is set to a reasonably high amount (in this study 1601 points are used) to improve precision. After the NA is

calibrated, device is placed onto the SUSS-Microtech test system. Probes are attached to electrodes as illustrated in Fig. 3.2(b). S-parameters are measured and saved in s2p file format. Equivalent electrical parameters are calculated using the measured magnitude and phase data. The saved s2p file is used to characterize a black-box in ADS simulation. The relative scattering parameter is chosen according to the network analyzer input.

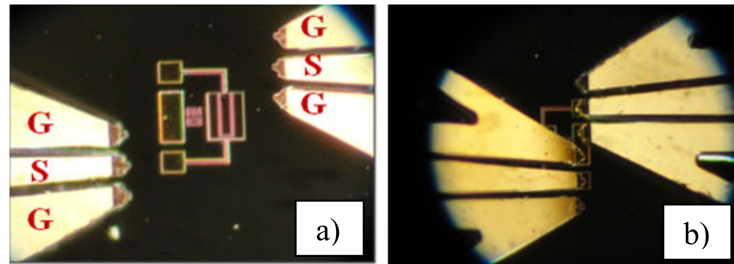

Figure 3.2: a) DUT and probe source-ground notation. b)Two-port measurement configuration

3.2 One Port-TPoS Equivalent Circuit Modeling

The single port TPoS and its NA connection is shown in Fig. 3.3(a). Middle electrode is connected to the test environment. The elements R_m, L_m, C_m represent the motional arm; also C_0 represents the parasitic capacitance between the top and bottom electrodes. At the resonance frequency, the reactive components of the motional arm cancel out, so the DUT behaves as a pure resistive component.

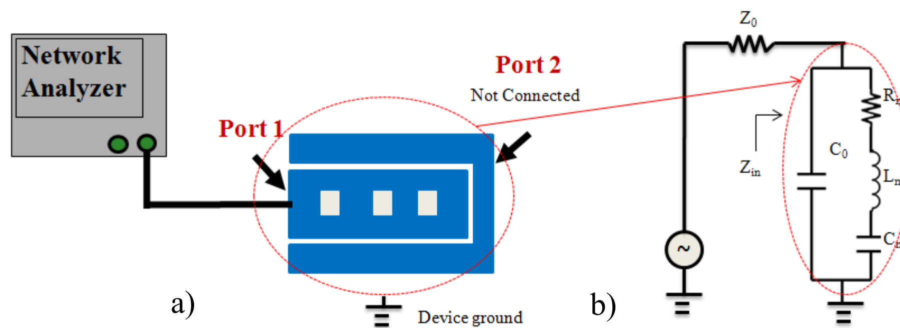

Figure 3.3: a) One-port device testing configuration b) Equivalent circuit diagram

The scattering parameter S_{11} which is also known as reflection coefficient is defined as;

$$\Gamma = S_{11} = \frac{Z_{in} - Z_0}{Z_{in} + Z_0} \tag{3.1}$$

Z_{in} is the input impedance and Z_0 is the network termination as it is given in Fig. 3.3(a). C_0 shows relatively high impedance (in the range of few hundreds of kΩ to MΩ). Therefore, C_0 is neglected at this point for motional arm parameter extraction. The complex impedance of the device is calculated by the reflection coefficient and the equation is given as;

$$Z_{in} = Z_0 \frac{1 + S_{11}}{1 - S_{11}} \tag{3.2}$$

In our network, a 50 Ω termination is used for Z_0. The data is collected for impedance magnitude and phase from the network analyzer. The motional resistance (R_m) is determined at the resonance frequency where minimum absolute value is observed. The challenge in one-port design is that the quality factor can not be directly measured. Quality factor is calculated by the derivation of the impedance with respect to frequency. Quality factor for one port model is given in Eq. 3.3.

$$Q = \frac{1}{2} f_r \frac{\partial \angle Z}{\partial f} \tag{3.3}$$

where f_r is the resonance frequency and $\angle Z$ is the argument of complex impedance in radians. The quality factor is derived from phase data according to the Eq. 3.3. The parasitic capacitance C_0 is also calculated by the expression;

$$C_0 = \frac{A\, \varepsilon_0\, \varepsilon_r}{d} \tag{3.4}$$

ε_0 and ε_r are permittivity and dielectric constant of AlN respectively. The expressions for L_m, C_m are given as in Eq. 3.5 and Eq. 3.6.

$$L_m = \frac{QR}{2\pi f_r} \tag{3.5}$$

$$C_m = \frac{1}{(2\pi f_r)^2 L} \tag{3.6}$$

Next, the calculated circuit model is simulated in ADS. The measured S-parameter data is simulated separately in ADS as well. The final equivalent electrical model is reported after curve fitting and results are given in Table 3.1 and Fig. 3.7.

3.2.1. Results for One-port Parameter Extraction

Directly measured frequency response is given in figure 20 with the wafer specifications. Center frequency is measured as 27.506 MHz for the device under test.

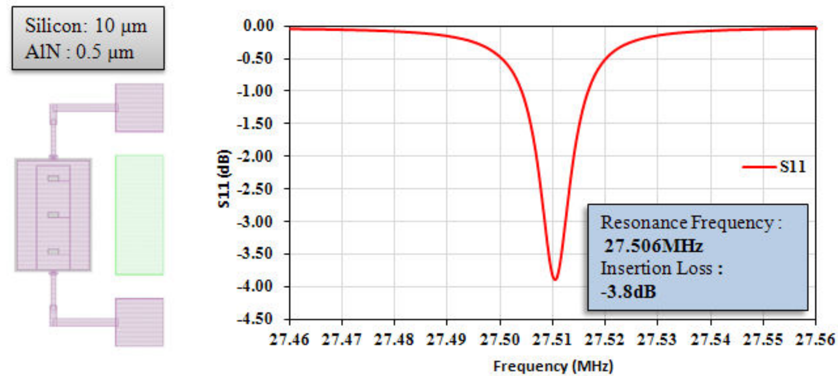

Figure 3.4: One-port device stack dimensions and frequency response

The device is fabricated on to a 10 µm silicon substrate and 0.5 µm AlN piezoelectric film is deposited. Measurement is taken from the middle electrode.

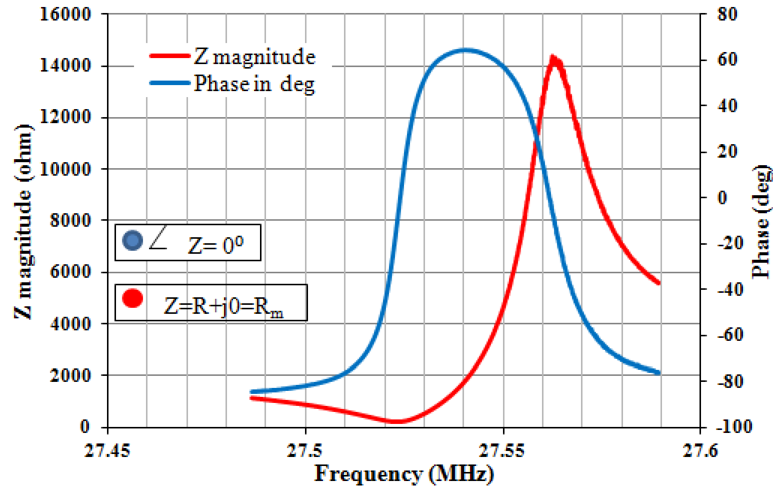

Figure 3.5: Device motional impedance magnitude and phase response

Fig. 3.5 shows the logarithmic magnitude and phase plot of the impedance. The motional resistance is extracted by determining the minimum impedance point. Quality factor is calculated by the derivation of the Z phase with respect to the frequency which is given in Eq. 3.3. After the R_m and the Q is determined the L_m and the C_m is calculated. The calculated BVD model is simulated in ADS software. Another simulation block is characterized with the measured S1p data and given in Fig. 3.6.

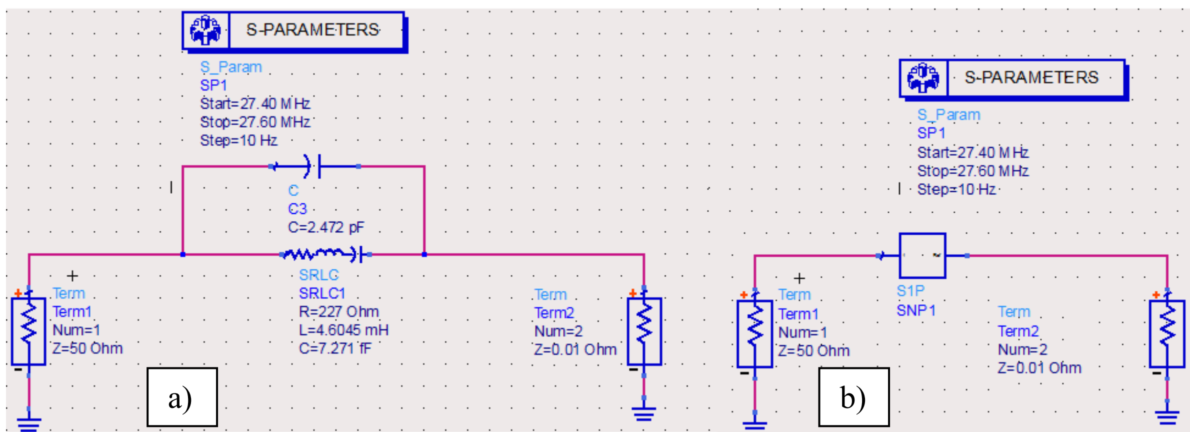

Figure 3.6: a) S-parameter simulation diagram with calculated parameters b) S-parameter simulation diagram with the extracted s1p file from network analyzer

Both simulation results are matched by curve fitting and the final circuit model is achieved in Fig. 3.6(a). The curve fit S11 plot and final BVD model parameters are given below in Table 3.1 and Fig. 3.7.

One-port BVD Model Parameters				
Rm (Ω)	Q	Cm (fF)	Lm(mH)	Co(pF)
227	3332	7.271	4.604	2.472

Table 3.1: One-port calculated equivalent model for the device under test

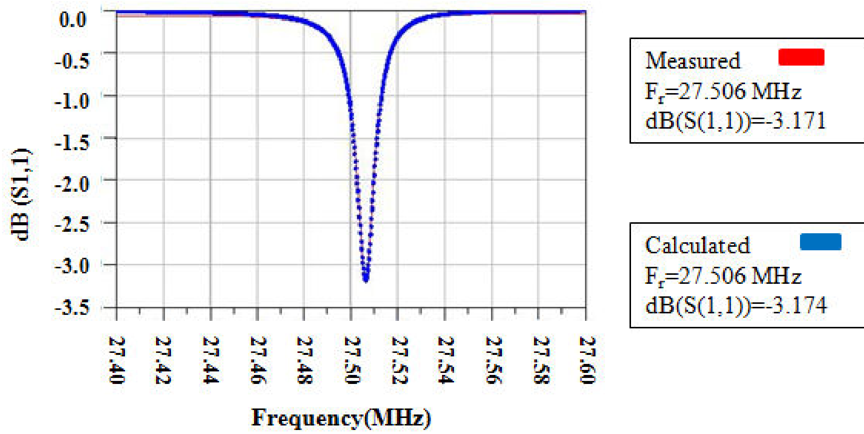

Figure 3.7: Reflection parameter curve fit with finalized BVD circuit model

3.3 Two Port-TPoS Equivalent Circuit Modeling

BVD circuit for two-port model is developed in terms of resonance frequency, insertion loss and quality factor which are directly measured by the network analyzer. Device testing schematic is given in Fig. 3.8. It can be seen that the difference from one-port design is that both the middle electrode and the fork electrode are connected to the terminations. In two-port configuration, the input and the output are electrically isolated from each other [35]. This isolation forms a resonant transformer which can be an advantage for certain applications.

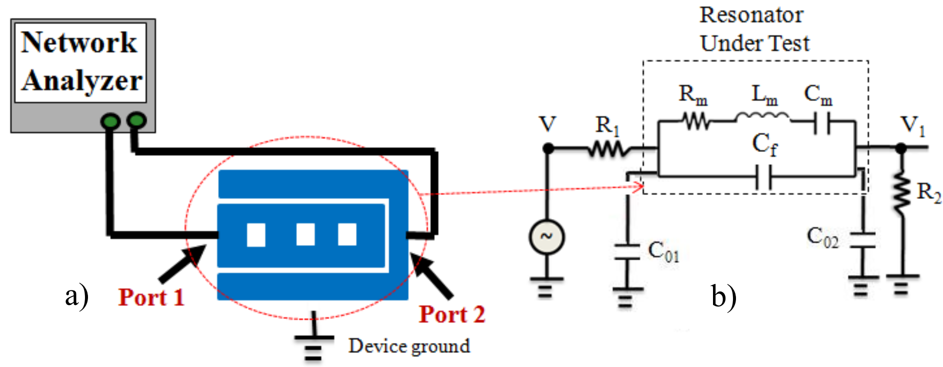

Figure 3.8: a) Two-port device testing configuration b) Testing configuration equivalence circuit diagram

The testing configuration which is given in Fig. 3.8(a) can be modeled as it is given in Fig. 3.8(b). The additional capacitors are seen in Fig. 3.8(b) compare to the one-port model. C_f is the feed-through capacitance which is caused by the interaction between middle and fork electrodes. C_{01} and C_{02} are intrinsic capacitances exist between top and bottom electrode. The intrinsic capacitances present very high impedance compared to terminations. Therefore, they will be assumed as negligible. However, they will be calculated separately and will be placed into the final model. Also at resonance the resonator becomes resistive and the circuit can be further simplified as it is given in figure25.

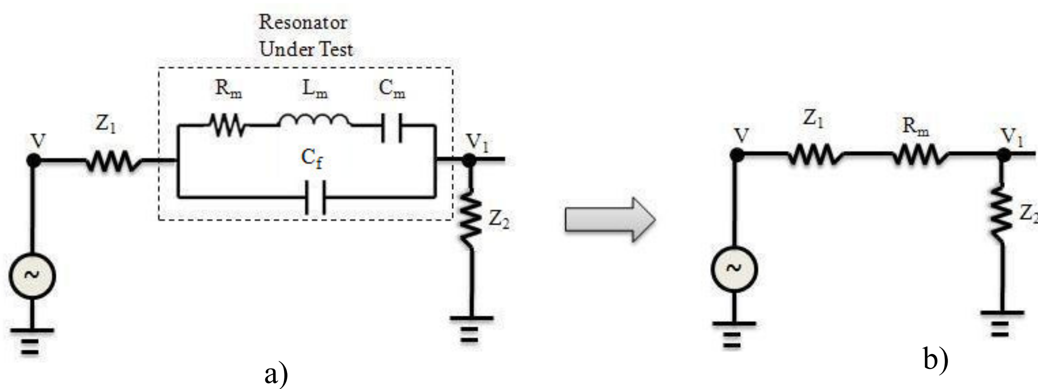

Figure 17: a) Testing configuration equivalence circuit diagram b) Simplified equivalence circuit at resonance frequency in order to derive motional resistance

Motional resistance R_m is calculated from the (V_1/V) at the resonance frequency. Insertion Loss (IL) is given as;

$$\text{IL (dB)} = 20\log_{10}|S_{21}| \tag{3.7}$$

$$S_{21} = \frac{2 * V_1}{V} \tag{3.8}$$

$$A_v = \left(\frac{V_1}{V}\right) = \frac{Z_2}{50 + R_m + 50} \tag{3.9}$$

Z_1 and Z_2 represent the 50 Ω embedded resistance of the network analyzer. Using 50 Ω terminations and using the given equation above the insertion loss can be expressed as;

$$\text{IL (dB)} = 20\log_{10}\left|\frac{2 * 50}{50 + R_m + 50}\right| \tag{3.10}$$

$$R_m = 100\left(10^{\frac{-IL}{20}} - 1\right) \tag{3.11}$$

Once the motional resistance expression is derived, next the equivalent circuit elements can be calculated. A summary for two-port equivalent BVD circuit extraction is given below.

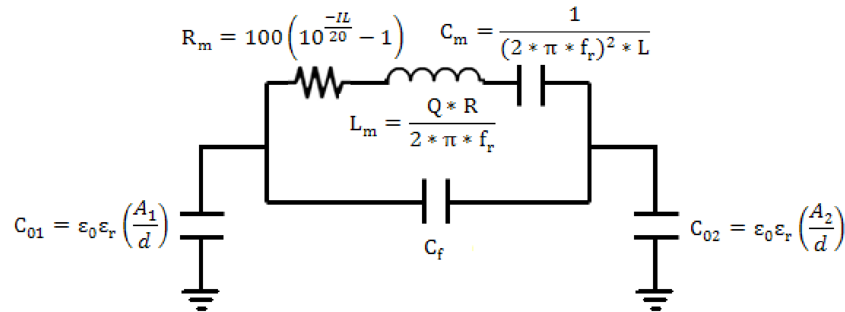

Figure 3.10: Two-port equivalent lumped circuit model

3.3.1. Results for Two-port Parameter Extraction

The same 27MHz device is used for two-port modeling which has been studied in previous chapter for one-port equivalent circuit extraction. Fig. 3.11 shows the frequency response of the device. Device presents relatively high quality factor and good selectivity.

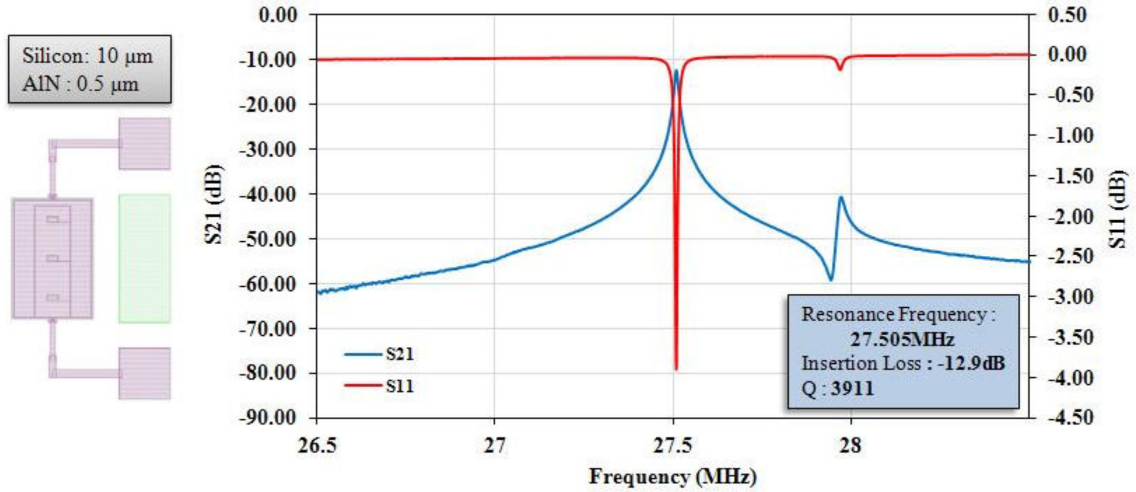

Figure 3.11: Two-port device stack dimensions and frequency response

Table 3.2 shows the results for calculated electrical circuit parameters by using equations given in Fig. 3.10. However, due to the assumptions the calculated parameters will not give the actual device equivalence parameters. Device two-port equivalence circuit graph which has been simulated in ADS is given in Fig. 3.12.

Two-port BVD Model Parameters						
R_m (Ω)	Q	C_m (fF)	L_m(mH)	C_f(fF)	C_{01}(pF)	C_{02}(pF)
342	3911	4.321	7.748	5	2.472	3.333

Table 3.2: Two-port finalized equivalent electrical model for TPoS

The simulated frequency response is matched with the directly measured device frequency response. The circuit parameters after the curve match are reported as device equivalent BVD circuit model. The optimization of these parameters with curve fitting is

important in order to receive correct bandwidth and the quality factor which are vital characteristics to be matched.

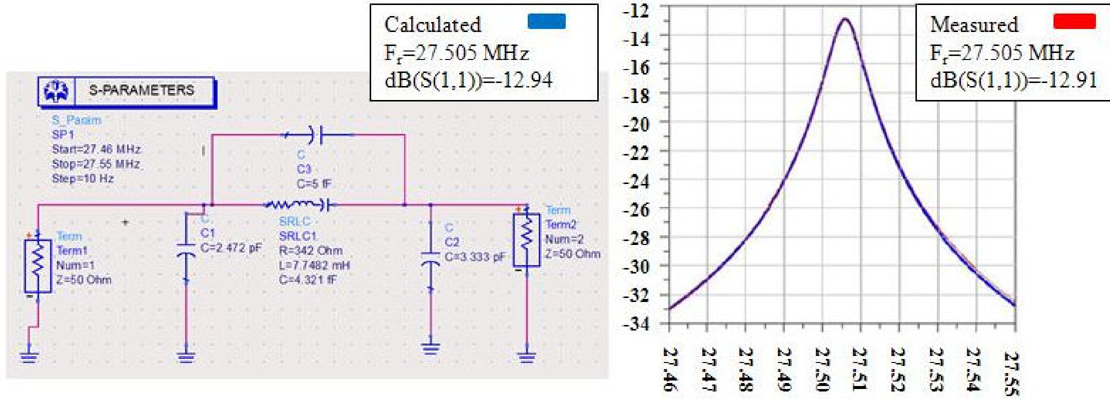

Figure 3.12: Two-port finalized BVD circuit model after curve fit

Determined error between the calculated and the final reported circuit elements are less than 2 %. However, calculated parameters cannot present the final accurate model; it gives insight on device performance. Reported low motional resistance and high quality factor provide advantage for the following oscillator implementation of TPoS.

The devices reported in Table 3.3 belong to separate wafers. Since substrate thickness has a big impact on resonance behavior it is worth mentioning the wafer specifications for each device. 27MHz device is fabricated on 10 µm silicon with 0.5 µm AlN piezoelectric layer. 54 MHz device is fabricated on to a 25 µm silicon substrate with 0.5 µm AlN layer.

Resonance Frequency	**Motional Resistance Rm (Ω)**	**Motional Inductance Lm (mH)**	**Motional Capacitance Cm (fF)**	**Intrinsic Capacitance (fF)**
27MHz	342	7.748	4.321	5
54MHz	1050	36.703	0.246	0.1

Table 3.3: TPoS equivalent electrical model for different center frequency devices

3.4. Effects of device geometry on Resonance Characterization

Two different designs are examined in this section. One design with etched holes is named as perforated electrode. The other design which has no holes on its electrodes is named as continuous electrodes. In the case of resonators that have been used in this study, the function of etched holes through middle electrode arises from lithography concerns. However, etched holes would also reduce the mass loading in device. The mechanical characteristics of the device would change as a result of mass loading and stiffness. Thus, frequency response variations are expected by mechanical changes (Eq. 2.2). Since MEMS mechanical and electrical behaviors are dependent, the change in mechanical characteristics would cause variation in electrical characteristics as well.

The effects of holes, which are etched on middle electrode, are studied from different point of views. First of all, thechange in frequency response and the change in equivalent electrical circuit elements are studied for perforated and continuous electrode. Secondly, three identical perforated devices with different holes area are tested. It is noted that the area of holes cause changes in device characteristics additionally. At last, the substrate thickness effect on device performance is investigated. The measurements are taken for identical devices which are fabricated on 5µm and 25µm Silicon substrates.

3.4.1. Perforated and Continuous Electrode

The effect of holes on device performance is studied for 27MHz and 54MHz devices which are introduced in Fig. 3.13. The 27 MHz devices (Device 01 and 06) and 54MHz resonance frequency devices (Device 26 and 27) are fabricated on the same wafer which has a 0.5 µm AlN piezoelectric layer on 25µm silicon substrate.

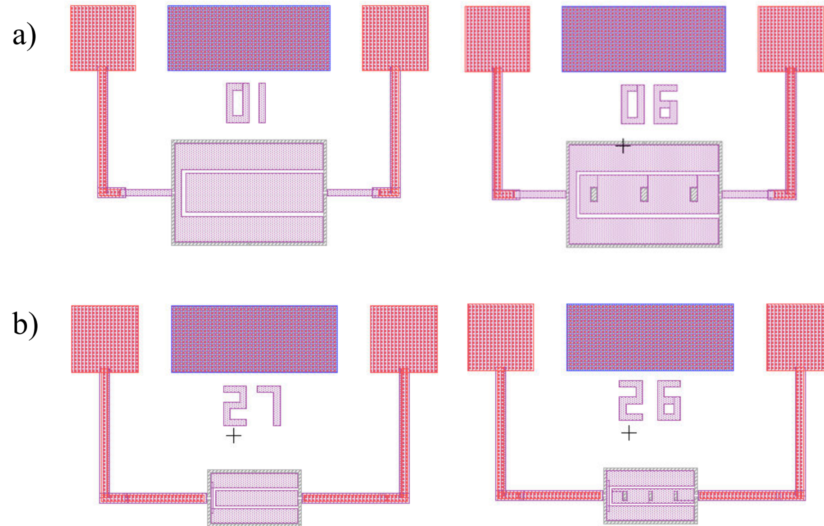

Figure 3.13: a) Identical devices for 27MHz with continuous electrode (01) and perforated electrode (06). b) Identical devices for 54MHz with continuous electrode (27) and perforated electrode (26).

Device	A1-port1 area(μm^2)	A2-port2 area(μm^2)	
01	32907.95	26804.75	**Port 1 (A1):** The port with two fingers
06	32907.95	26078.75	
26	21046.25	17616.25	**Port 2 (A2):** The port with one finger
27	21046.25	17868.25	

Table 3.4. Device surface dimension in order to confirm the devices are identical in their own group (for same resonance frequency)

The dimensions of two identical devices for the 54 MHz and the 27 MHz devices are given in Table 3.4. Device 06 is perforated and device 01 is continuous electrodes. The processed 4 inch wafer consists of 20 die. The data for each device is collected from at least 10 die. In other words, the same device is tested on minimum 10 different die. This data is used to insert error bars which give the information of performance range for each design. The same method is repeated for device 26 and device 27. Fig. 3.14 shows the chance in frequency for 27 MHz devices. Also the resonance frequency behavior for 54 MHz devices is given in Fig. 3.15.

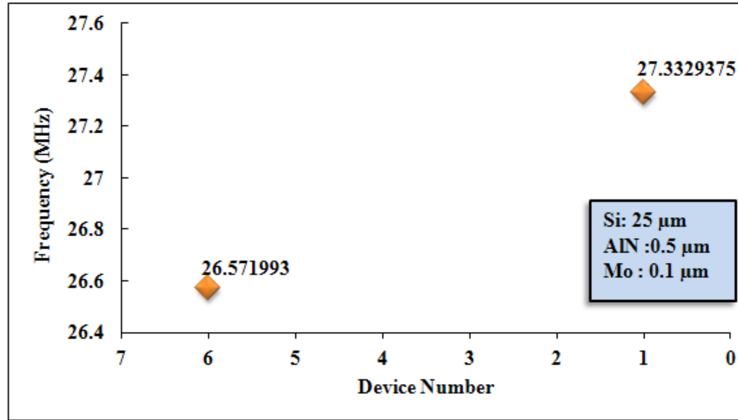

Figure 3.14: Resonance frequency behavior of continuous and perforated electrode for 27 MHz TPoS

It can be seen from the Fig. 3.14 and Fig. 3.15 that that the etched holes into the middle electrode cause the resonance frequency to shift downward. The resonance frequency has shifted downward by approximately 2 % in perforated electrode design. The amount of frequency shift is almost equal for both 27 MHz and 54 MHz in percentage.

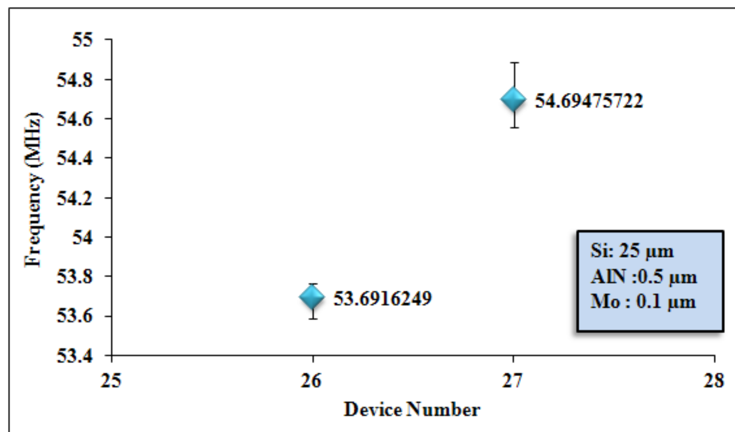

Figure 185: Resonance frequency behavior of continuous and perforated electrode for 54 MHz TPoS

An important finding is observed that the quality factor and the loss show improvement with perforated electrode at 27 MHz. However, the opposite effect is noted for 54 MHz devices. In 27 MHz devices, insertion loss has decreased by 8 %. On the other hand, in 54 MHz devices, insertion loss is increased by 18 % with perforated design.

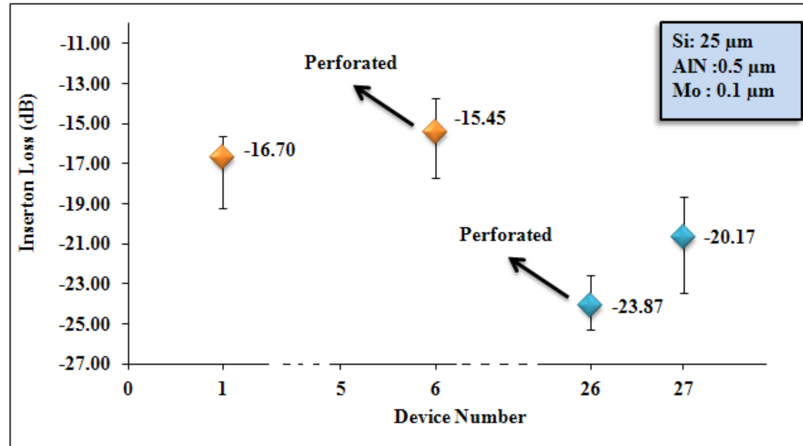

Figure 3.16: Insertion loss behavior of continuous and perforated electrode for 27 MHz and 54 MHz TPoS

In addition to this, quality factor is increased by 34 % with the 27 MHz perforated design. However, 20 % decrease is observed in quality factor for 54 MHz perforated devices. The results are given in Fig. 3.17.

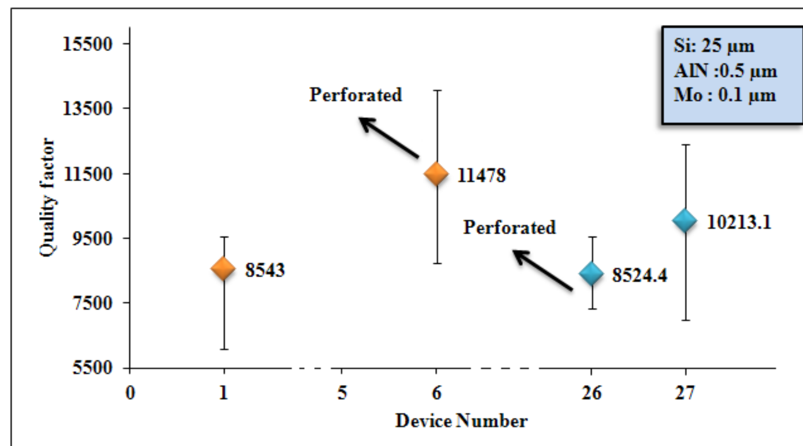

Figure 3.17: Quality factor behavior of continuous and perforated electrode for 27 MHz and 54 MHz TPoS

As it is mentioned previously, changes in mechanical characteristics as a consequence of the etched holes in the middle electrodes would change electrical characteristics also. The equivalent electrical model elements are extracted for both perforated and continuous electrodes. The comparison is given in Fig. 3.18, Fig. 3.19 and Fig. 3.20.

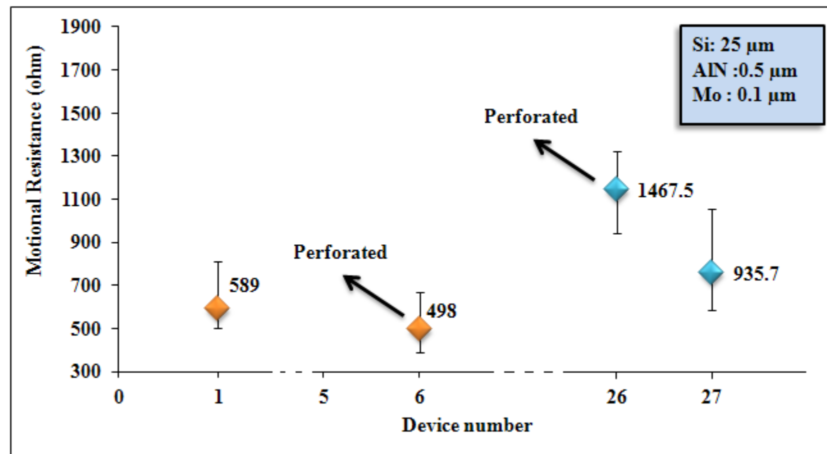

Figure 3.18: Motional resistance behavior of continuous and perforated electrodes for 27 MHz and 54 MHz TPoS resonators

Lower motional resistance is achieved with the perforated design for 27 MHz devices. On the other hand, motional resistance increases with perforated design for 54 MHz devices. Results for the identical device groups (devices 1-6 and devices 26-27) are presented in Fig. 3.18. Furthermore, the motional capacitance and the motional inductor behavior are given in Fig. 3.19 and Fig. 3.20.

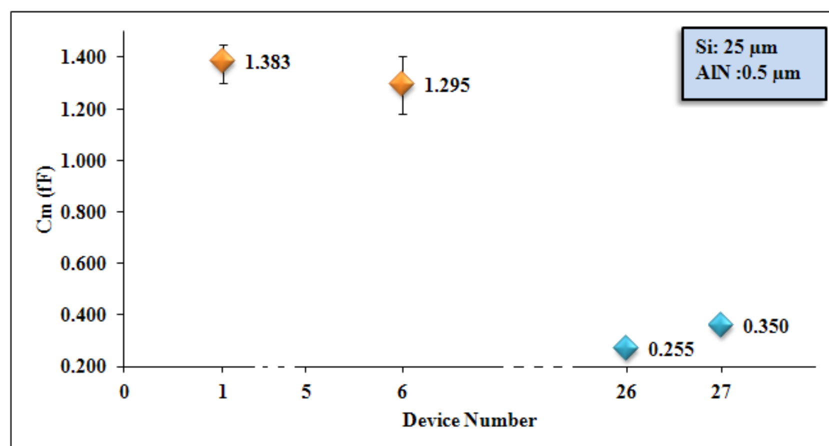

Figure 3.19: Motional capacitance behavior of continuous and perforated electrodes for 27 MHz and 54 MHz TPoS resonators

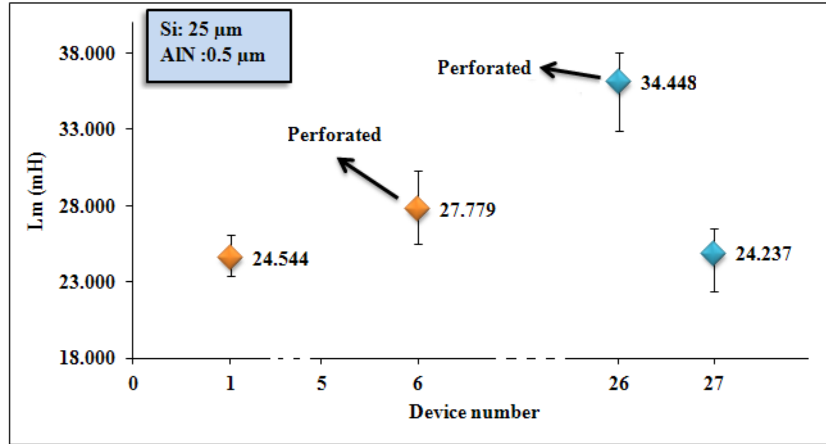

Figure 3.20: Motional inductor behavior of continuous and perforated electrodes for 27 MHz and 54 MHz TPoS resonators

Fig. 3.19 and Fig. 3.20 demonstrate that the perforated design cause a decrease in motional capacitance but also an increase is observed in motional inductance.

3.4.2. Perforated Electrode with Different Hole Dimensions

Three identical devices with different hole dimensions have been tested to observe the effect of miscellaneous holes on the frequency response and on the electrical characteristics. Three devices which are fabricated with 1µm AlN on 5µm silicon substrate are tested. The device schematics are given in Fig. 3.21 and the hole area for each device is listed in Table 3.5.

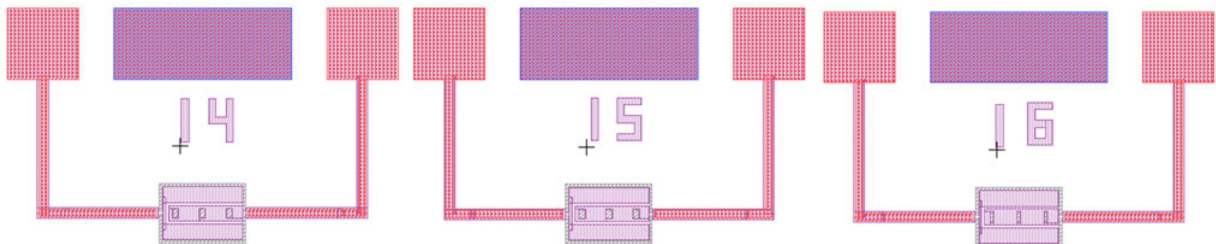

Figure 3.21: Identical devices under test with different hole dimensions

Device	A1-port1 area(μm^2)	A2-port2 area(μm^2)	Hole Area
14	20352.75	17256.75	112
15	20352.75	17172.75	140
16	20352.75	17304.75	96

Table 3.5: Dimensions for identical devices with different hole areas

The area reported in Table 3.5 is given only for one hole. Each middle electrode consists of three etched holes. Fig. 3.22 shows that the frequency shifts to downward by the increased hole area.

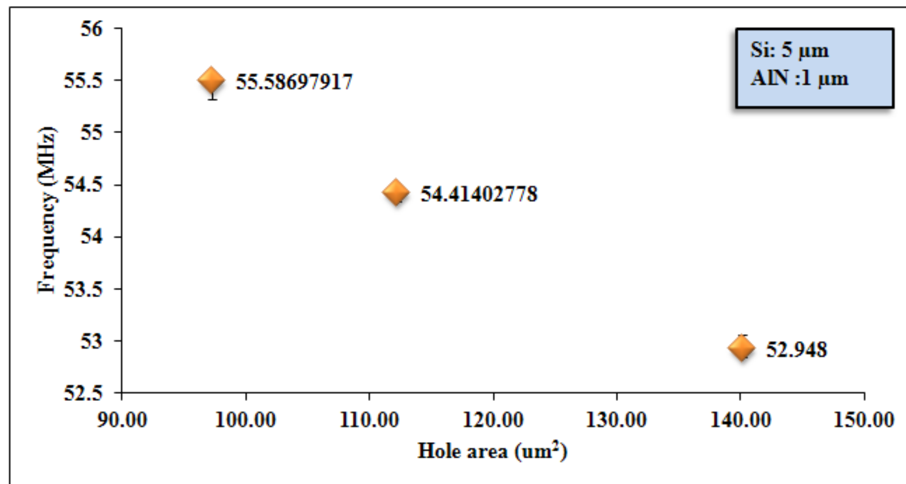

Figure 3.22: Frequency shift in perforated design for different hole area

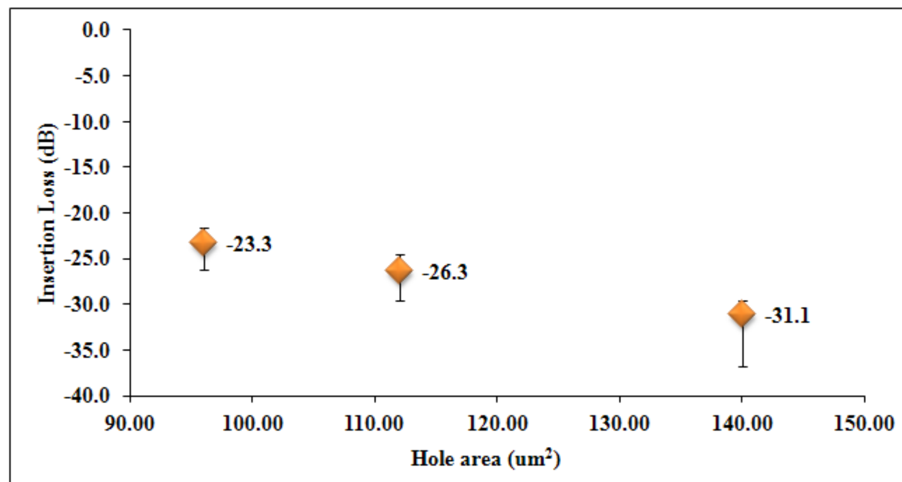

Figure 3.23: Insertion loss behavior in perforated design for different hole area

Insertion loss is increased by the increased hole area which also means that the motional resistance would increase as well. Fig.3.23 and Fig. 3.25 can be compared in order to comment on the relation between two characteristics. Motional resistance is increased by 62 % and presented in Fig. 3.25.Moreover, the quality factor decreases dramatically for larger holes. Fig. 3.24 shows approximately 50 % decrease in quality factor.

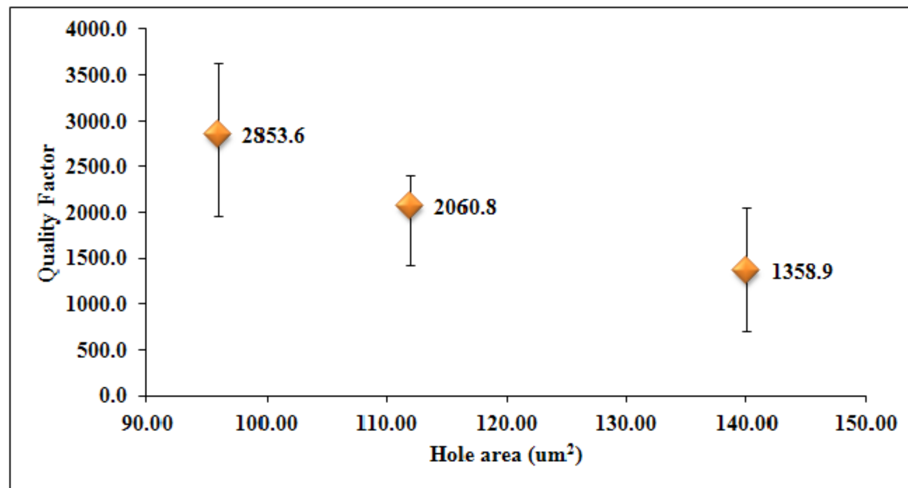

Figure 3.24: Quality factor behavior in perforated design for different hole area

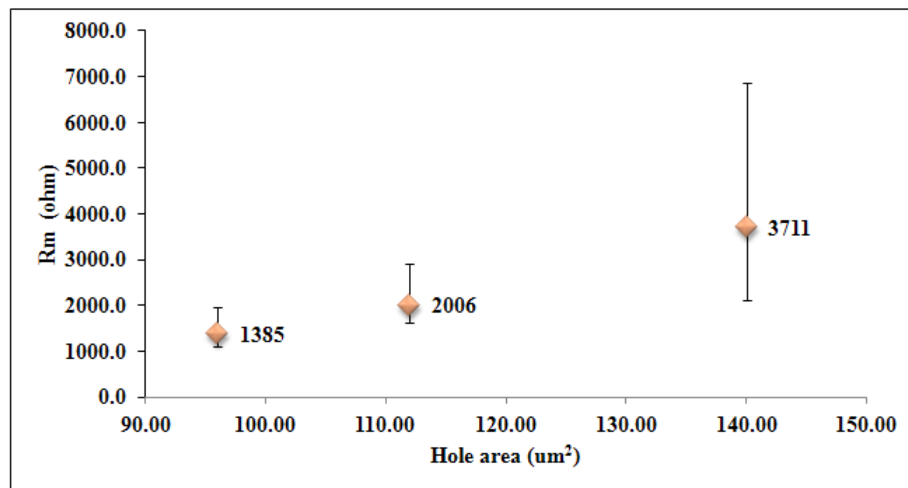

Figure 3.25: Motional resistor behavior in perforated design for different hole area

Finally, the reactive motional elements behavior is given in Fig. 3.26 and Fig. 3.27.

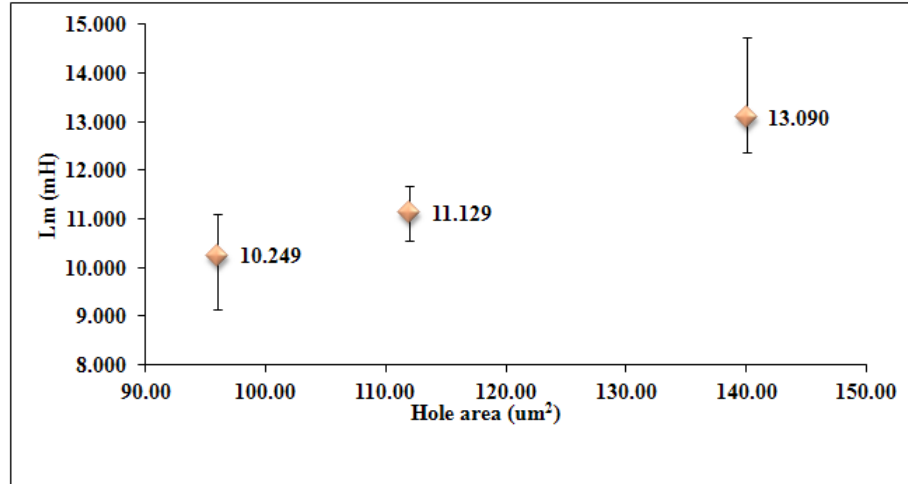

Figure 3.26: Motional inductor behavior in perforated design for different hole area

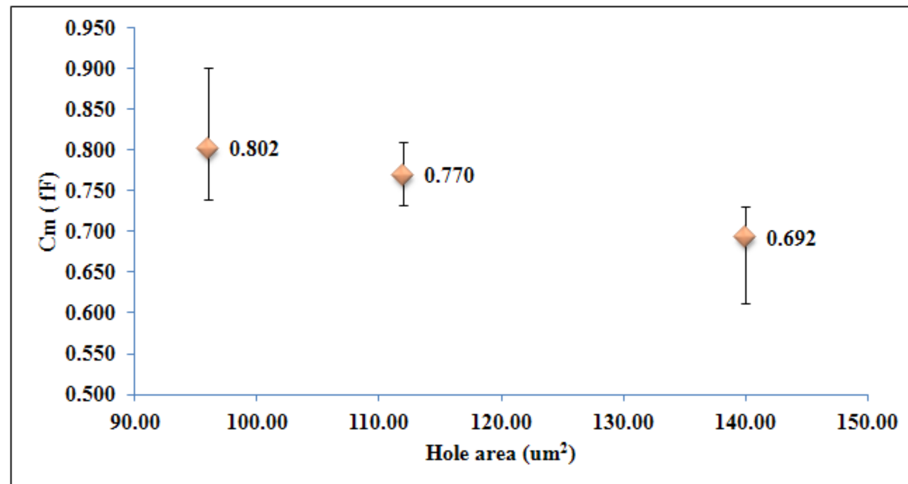

Figure 3.27: Motional capacitance behavior in perforated design for different hole area

3.4.3. Substrate Thickness Effect on Resonance Behavior

TPoS resonators are fabricated on a substrate which is made of low loss material. It is already introduced in previous sections that the TPoS resonance characteristics are under influence of substrate thickness. The devices that have been tested in this study are fabricated on silicon substrate. In this section, the change in the resonance frequency response and the electrical characteristics are studied in terms of substrate thickness.

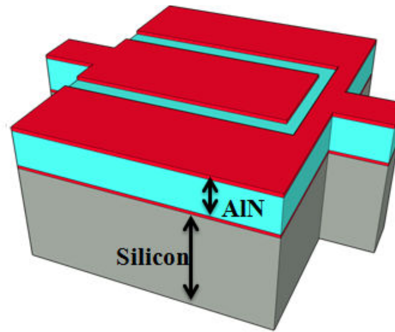

Figure 3.28: TPoS resonator multilayer schematic

Fig. 3.29 shows that the resonance frequency is shifted upwards by approximately 4.5 % as a result of %400 increase in silicon thickness. The given resonance frequency expression (equation 2.2) in section 2 shows that center frequency is inversely proportional to the effective mass. Therefore, it is an expected result that the resonance frequency would increase by decreased substrate thickness (decreased effective mass). Also an additional finding noted here is that the resonance behavior for both perforated and continuous electrode designs are similar. Thus, the substrate thickness influences the device response regardless of its design structure.

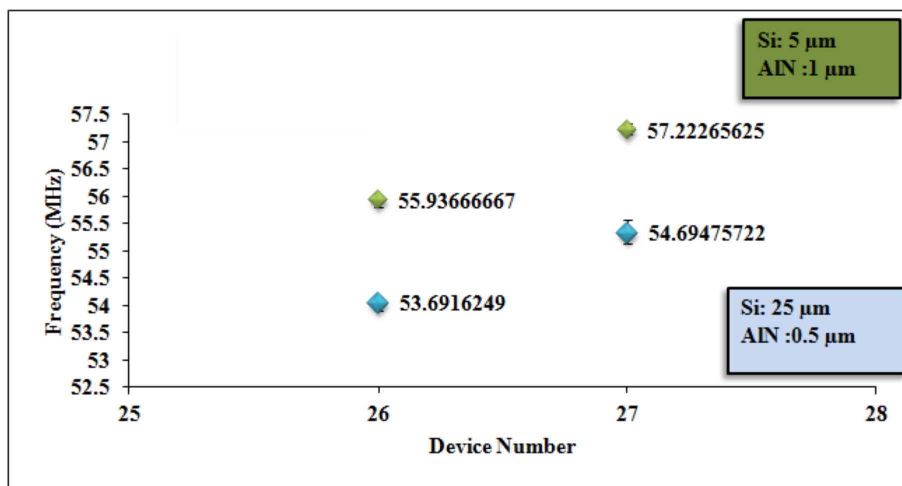

Figure 3.29: The change in resonance frequency in terms of substrate thickness in TPoS resonators

No significant change is observed in the insertion loss. However, the error bars show that the devices fabricated on 25 μm silicon behaves more consistently. The approximate change in loss stays under 1 %. The motional resistance follows exactly the same behavior and the percent change in motional resistance is noted approximately 2 %.

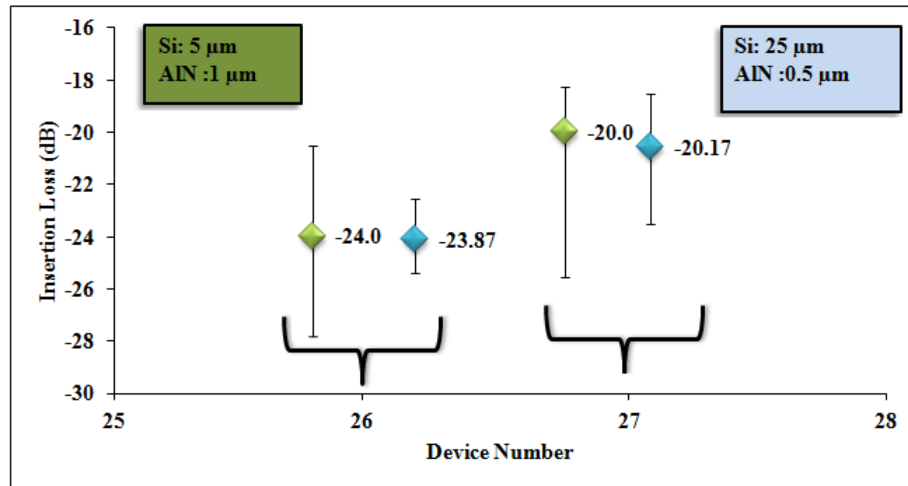

Figure 3.30: The change in insertion loss in terms of substrate thickness in TPoS resonators

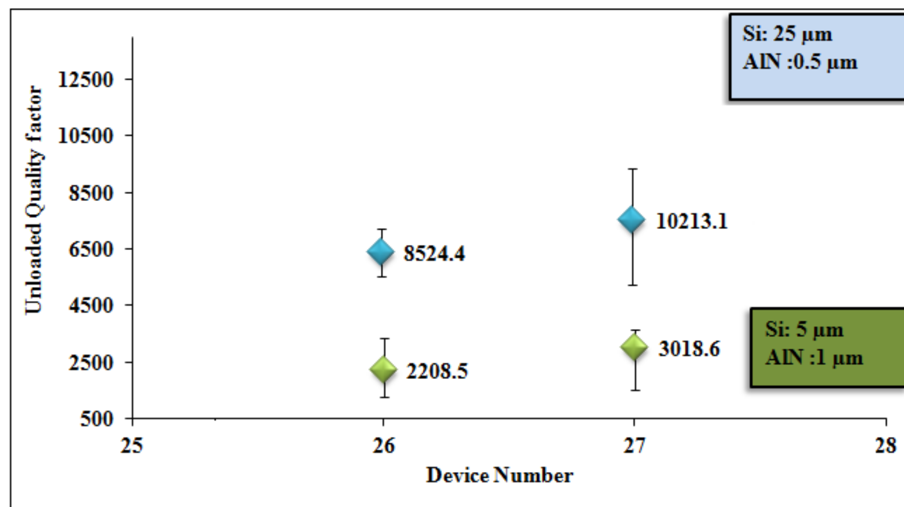

Figure 3.31: The change in quality factor in terms of substrate thickness in TPoS resonators

A dramatic change is noticed in quality factor. The device quality factor is increased by 290 % and 240 % in perforated and continuous electrode respectively with increased

substrate thickness. However, the trade-off between the quality factor and the power handling limits the maximum thickness that can be fabricated according to the desired application aspects. TPoS power handling is inversely proportional to the quality factor. The increased quality factor would lead nonlinearity and the device linear working regime becomes narrower [30].

CHAPTER IV

TPoS OSCILLATOR

Oscillator circuits are widely used in electronics to produce reference signal for electronic systems. In this chapter colpitts oscillator topology is studied. TPoS resonator is used as core element for the oscillator designs. First, the TPoS resonator equivalent circuit is extracted by the method which has been introduced in chapter 3. Later on, colpitts oscillator is demonstrated with the relevant TPoS resonator. The simulation and real-time application is presented. Implemented oscillator jitter results are reported. Also the same circuit is tested with the crystal resonator and the performance difference between TPoS and the crystal is discussed.

4.1 TPoS- Colpitts Oscillator

Colpitts oscillator is choosen for this TPoS application because of its simplicity and it is capable of achieving very low phase noise. However, achieving sufficient negative resistance at high frequency operations is challenging with colpitts oscillator due to the miller effect which is introduced in section 2.4.3. At high frequencies, the miller capacitances reduce the negative resistance which is critical for oscillation start-up. In this study, modified colpitts circuit topology is used with a collector inductor and an emitter inductor.

4.2 TPoS Resonator Equivalence Model for Colpitts Oscillator

In this study, the TPoS resonator is used as a one-port device. In order to increase transduction area, both electrodes are connected to the oscillator input. The purpose with increasing transduction area is decreasing the effective motional resistance of the device.

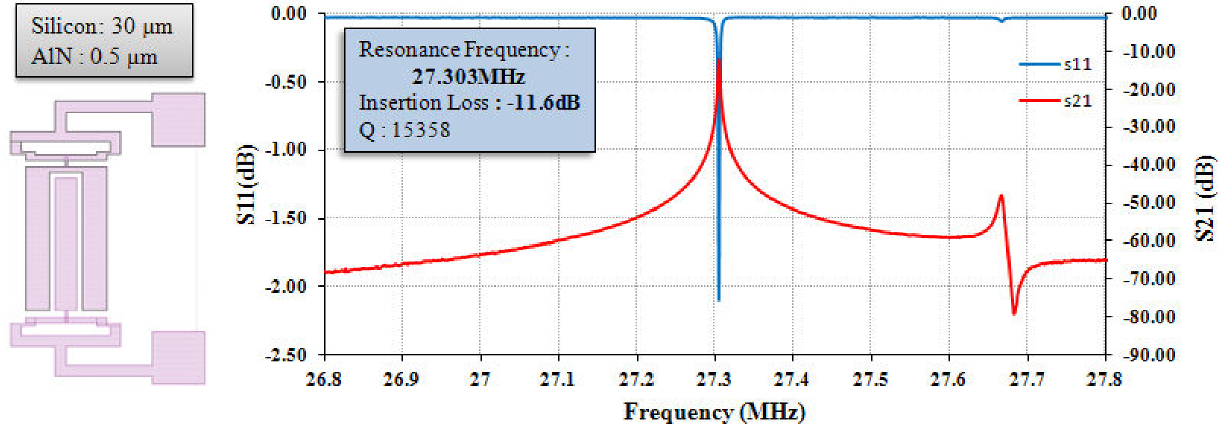

Figure 4.1: Frequency response and device schematic of the TPoS used in colpitts implementation

The device diagram and the frequency response of the TPoS is given in Fig. 4.1 which is used for colpitts oscillator design in this study. The equivalent BVD circuit elements are listed for one-port and two-port model of relevant resonator Table 4.1 and Table 4.2.

Model for connected middle electrode			
R_m (Ω)	L_m (mH)	C_m (fF)	C_0 (pF)
385	31.965	1.063	5.663

Table 4.1: One-port BVD elements of TPoS for colpitts oscillator implementation

Model for connected two electrodes					
R_m (Ω)	L_m (mH)	C_m (fF)	C_0 (fF)	C_1 (pF)	C_2 (pF)
281	34.253	0.992	37	5.663	8.321

Table 4.2: Two-port BVD elements of TPoS for colpitts oscillator implementation

4.3 Colpitts Oscillator Circuit Simulation

The colpitts oscillator circuit diagram is given in Fig. 4.2. The circuit consists of two main parts that the resonator and the active circuit. The general purpose BJT transistor 2N2222A is used in the simulation. The effects of the circuit elements are investigated with Multisim simulation model in order to have a better insight on circuit behavior.

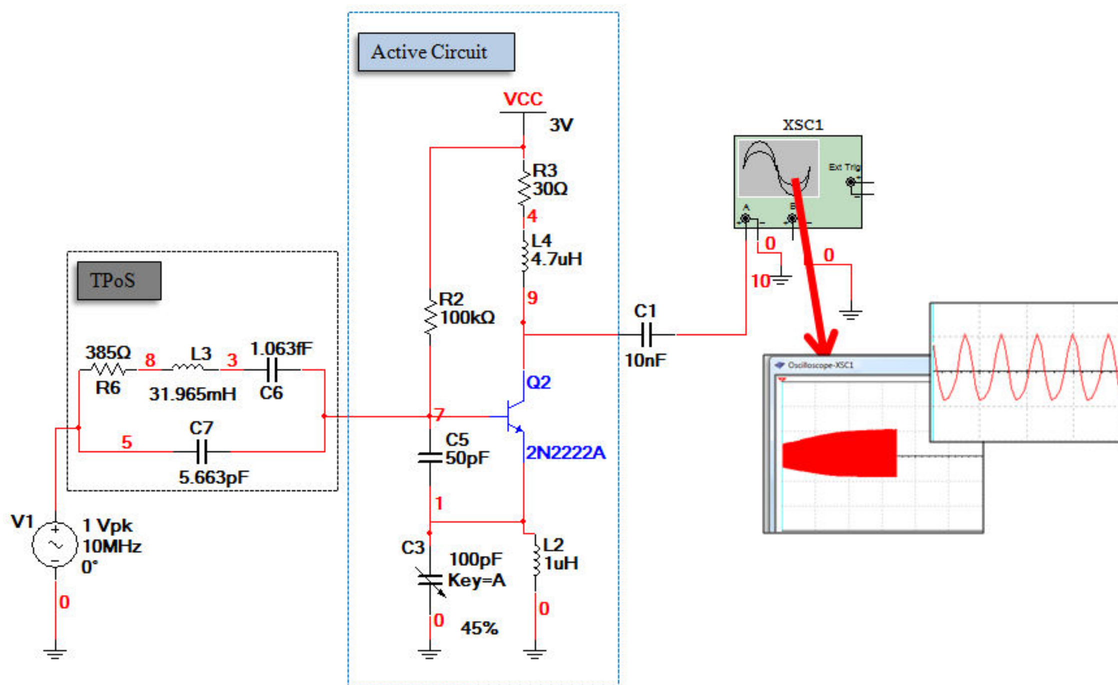

Figure 19.2: TPoS colpitts oscillator simulation model

3V bias voltage is applied to the transistor collector. Since the simulation environment does not include any nonlinear sources the circuit needs to be manually triggered. The alternating voltage with a very large damping factor (~10^7) is applied to provide necessary trigger. This alternative voltage will be damped fast due to damping factor so it has no influence on the circuit output.

The resistor R_2 is the bias resistor which mainly provides necessary bias to the circuit. The value for bias resistor is picked as 100kΩ. The R_2 has no big influence on performance. However, it should be large enough compare to the overall active circuit resistance so that very small current (few μA) flow through on R_2. Furthermore, bias resistor provide a negative feedback which stabilizes the bias point of BJT transistor [43].

The collector inductor L_4 provides essential loading and also it has direct effect on circuit gain condition [43]. The circuit gain for given configuration is proportional to the collector impedance. In the simulated model given in Fig 4.2, the oscillation is observed for the L_4 values between 3.3μH to 5.3μH. The value 4.7 μH is chosen for L_4 due to supplied sufficient gain for this particular condition. The given L_4 range is valid only for the condition that all the other element values are kept constant as it is stated in Fig 4.2. Considering the gain is also under influence of positive feedback (C_3 and C_5), the effective range for L_4 would change related to the change in positive feedback. According to [46], there is an optimum value for L_4 in order to achieve maximum negative resistance in colpitts oscillator active circuit. Although the chosen value 4.7 μH for L_4 doesn't necessarily present the optimum inductor value but it satisfies the necessary overall negative resistance for active circuit.

Furthermore, the inductor L_2 which is connected to transistor emitter reflects the oscillator power back to the base with providing high impedance. It is known that the input impedance at the transistor base depends on the emitter resistance [43]. The changes in emitter impedance affect the base current. Low base current leads a low drive level operation which would make the circuit power efficient [47]. Additionally, it is observed that optimum L_2 is under influence of the capacitive C_3 due to phase conditions.

A particular C_3 range is observed for each L_2 that the oscillation conditions are satisfied. For the specific model given in Fig 4.2, the operation range for C_3 is noted between 42pF to 48pF.

The positive feedback of the active circuit is the fundamental part in an oscillator. In the topology given in Fig 4.2, C_3 and C_5 form the positive feedback. The required gain is adjusted by the ratio between the feedback capacitances C_3 and C_5. The impedance of C_3 should be chosen less than the emitter impedance L_2. In this model, C_5 is set to 50pF and a variable capacitance is placed for C_3 in order to tune the circuit to provide enough loop gain. The output response for the colpitts oscillator given in Fig 4.2 is presented below in Fig 4.3.

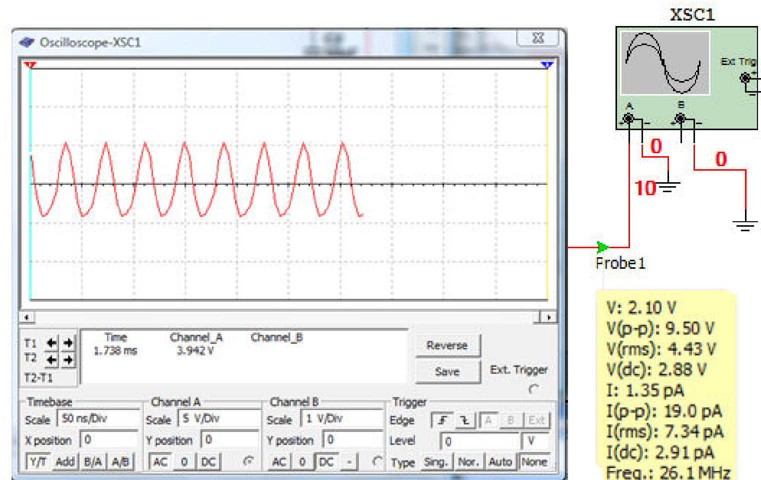

Figure 4.3: Colpitts oscillator output

The simulation circuit oscillates at 26.1MHz with approximately 9.5 V peak-peak output under 3V bias voltage. The jitter concept is associated with the oscillator noise which is explained in next chapter. Since the simulation environment is noise-free, the jitter is not reported in simulation results.

4.4.Colpitts Circuit Implementation

The oscillator model given in figure 49 is built on a PC Board. The circuit is tested with 27 MHz TPoS resonator and with 27 MHz crystal resonator. In crystal oscillator, ABL-27MHz-B2F crystal is used because of its availability which presents approximately 40Ω motional resistance. NTE123A general purpose bipolar-junction transistor is chosen because of its matched characteristics with the 2N2222A and also due to its availability as well. However, no response was observed in the output. Later the transistor is changed with a high frequency transistor BC847B. The oscillation is achieved with the high frequency transistor.

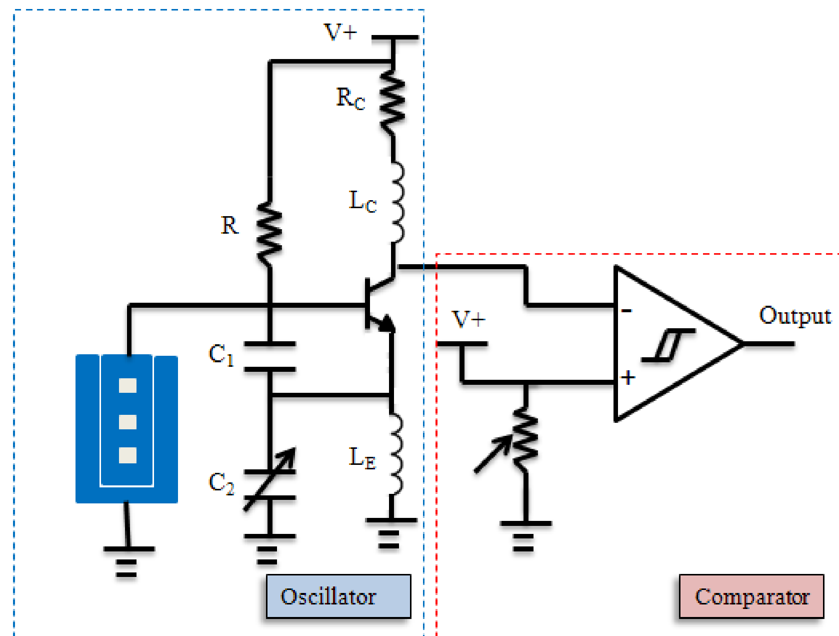

Figure 4.4: Colpitts implemented PC Board schematic20

Implemented circuit schematic is given in Fig. 4.4. The comparator part is added in the IC different than the simulation model. The comparator is connected with the purpose of

measuring the oscillator jitter. Necessary square wave for jitter measurement is provided by the comparator which is placed at the output of colpitts.

Noise sources cause variations in the output signal. Three main noise sources are categorized as thermal noise, shot noise and 1/f noise [52]. Jitter is described as time-domain measure of the oscillator circuit noise [53]. The period of the output signal varies due to the induced circuit noise components. Therefore, the variations in the zero crossing point of the waveform provide the noise information. Fig 4.5 can be referred as an oscillator jitter wave form. In order to calculate variations, a reference signal is required. In cycle-to-cycle jitter this reference is set to the average period. Oscilloscope is a type of electronic test instrument which is capable of taking time domain measurements. The variance of the output signal in each period is measured to the average period by the oscilloscope. The jitter can be measured through a sinusoidal wave as well. However, rapid changes of the square wave form at zero-crossing points improve the measurement precision. Therefore, the comparator is used after the colpitts oscillator in order to obtain more precise measurement

The jitter data is collected for TPoS and Crsytal resonators. Both electrodes of the TPoS resonator are wire bonded to the colpitts base. It is worth mentioning that the TPoS configuration in which the both ports are connected simultaneously to the base doesn't present the two-port operation of TPoS. The TPoS is still used as one-port device but the goal is to investigate if the enhanced transduction will improve the jitter. The observed lowest jitter for TPoS oscillator is noted as 8.67 ps under 5V supply voltage and it is given in Fig. 4.5.

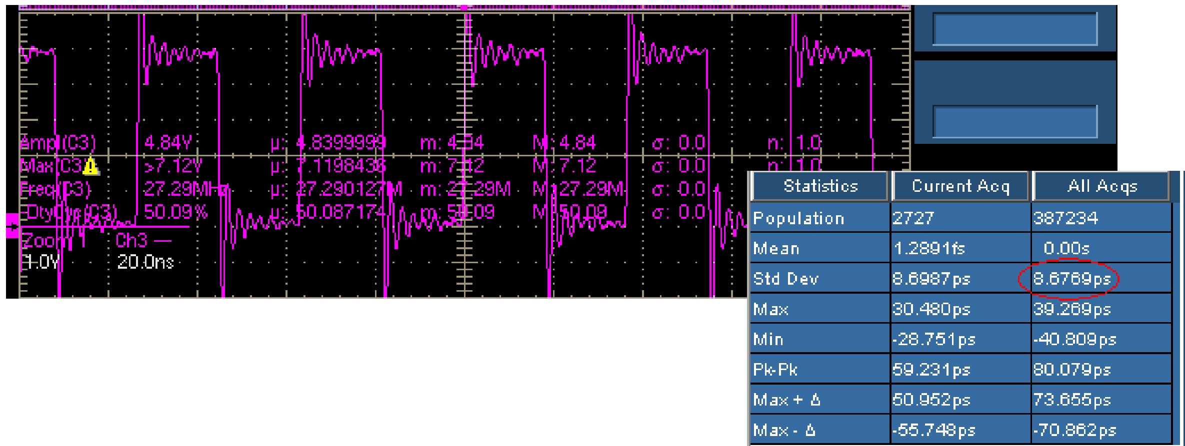

Figure 4.5: TPoS-Colpitts Oscillator jitter measurement

Furthermore, it is realized that connected two-port increase the operation range. The circuit oscillates down to 1.9 V supply voltage where it is limited by 2.4 in single-port connection.

At last, the crystal resonator is connected to the oscillator and the TPoS resonator is isolated from the circuit. The jitter is measured as 9.13ps under 4.8V supply voltage. According to the results received from both TPoS and crystal oscillator, TPoS resonator presents slightly better stability for each measurement. Fig. 4.6 shows the crystal jitter measurement results.

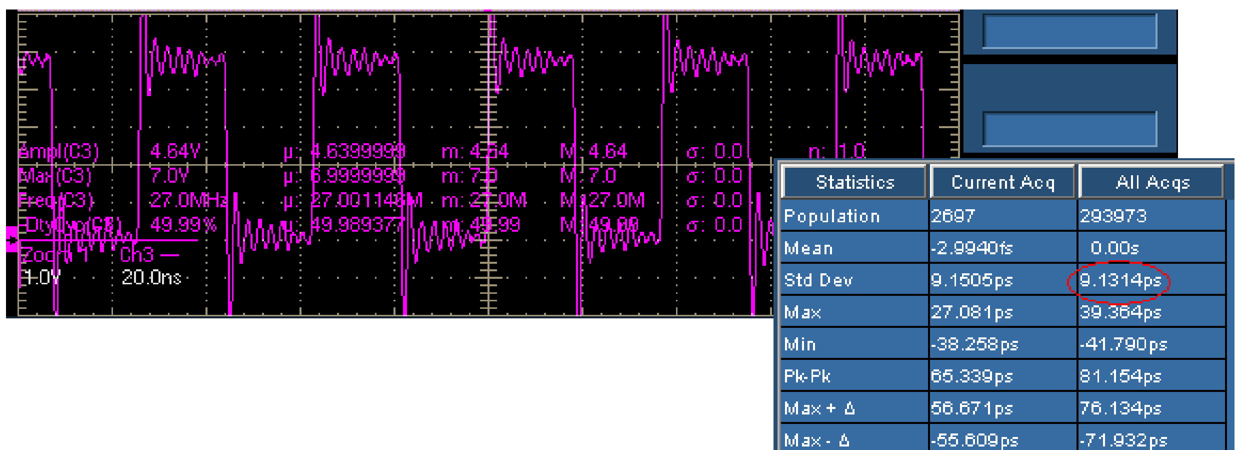

Figure 4.6: Crystal-Colpitts Oscillator jitter measurement

Moreover, it is observed that the jitter is improved by increased voltage. This is an expected result which is related to the output level of the circuit. The output level would be increased by increased supply voltage. Since the noise level is independent from the supply voltage, the noise level would stay the same where output level increases. Thus the increased signal to noise ratio leads more precise measurement and lower jitter is observed at the output.

Supply Voltage (V)	**Jitter for TPoS (ps)**	**Jitter for Crystal (ps)**
2	42.14	57.70
4	10.07	10.87

Table 4.3: Oscillator jitter improvement with increased voltage

CHAPTER V

CONCLUSION

Colpitts oscillator is known as highly stable oscillator circuit. However, their implementation with MEMS resonators is difficult due to the challenge of satisfying the sufficient negative resistance. In the present study, a modified colpitts oscillator was designed with the thin film piezoelectric on substrate (TPoS) resonators. Oscillation was achieved with the TPoS resonator and the quartz resonator. The jitter was reported as 8.67 ps for TPoS-Colpitts oscillator.

Moreover, thin film piezoelectric on substrate (TPoS) resonator equivalent electrical circuit parameters was extracted. The comparison of the resonance behavior for two different designs, perforated and continuous electrode, was demonstrated. An opposite resonant behavior was noted for the 27 MHz and the 54 MHz devices. The Q and insertion loss were improved with perforated design in 27MHz devices. However, lower Q and higher insertion loss was measured for 54 MHz devices. In addition, it was demonstrated that the larger hole dimension has increased the insertion loss and has decreased the quality factor. Furthermore, quality factor was increased dramatically by the increased substrate thickness.

REFERENCES

[1] G. E. Moore, "Cramming more components onto integrated circuits, Reprinted from Electronics, volume 38, number 8, April 19, 1965, pp.114 ff," *Solid-State Circuits Newsletter, IEEE,* vol. 20, pp. 33-35, 2006.

[2] G. E. Moore, "Progress In Digital Integrated Electronics [Technical literaiture, Copyright 1975 IEEE. Reprinted, with permission. Technical Digest. International Electron Devices Meeting, IEEE, 1975, pp. 11-13.]," *Solid-State Circuits Newsletter, IEEE,* vol. 20, pp. 36-37, 2006.

[3] H. Wan-Thai, "Resonator miniaturization for oscillators," in *Frequency Control Symposium, 2008 IEEE International*, 2008, pp. 392-395.

[4] SiTime, "MEMS Replacing Quartz Oscillators," 2009.

[5] C.S.Lam, "An Assesment of the Recent Developent of MEMS Oscillators as Compared with Crystal Oscillators," presented at the 2nd Symposium on Piezoelectricity, Acoustic Waves, and Device Applications, Hangzhou, Zhejiang, China, 2006.

[6] C. S. Lam, "A review of the recent development of MEMS and crystal oscillators and their impacts on the frequency control products industry," in *Ultrasonics Symposium, 2008. IUS 2008. IEEE*, 2008, pp. 694-704.

[7] L. Sheng-Shian*, et al.*, "Micromechanical "hollow-disk" ring resonators," in *Micro Electro Mechanical Systems, 2004. 17th IEEE International Conference on. (MEMS)*, 2004, pp. 821-824.

[8] W. Jing*, et al.*, "RF MEMS Resonators: Getting the Right Frequency and Q," in *Compound Semiconductor Integrated Circuit Symposium, 2007. CSIC 2007. IEEE*, 2007, pp. 1-4.

[9] W. Jing*, et al.*, "1.51-GHz nanocrystalline diamond micromechanical disk resonator with material-mismatched isolating support," in *Micro Electro Mechanical Systems, 2004. 17th IEEE International Conference on. (MEMS)*, 2004, pp. 641-644.

[10] R. Abdolvand and F. Ayazi, "Monolithic Thin-Film Piezoelectric-on-Substrate Filters," in *Microwave Symposium, 2007. IEEE/MTT-S International*, 2007, pp. 509-512.

[11] M. Rinaldi*, et al.*, "Reconfigurable CMOS Oscillator Based on Multifrequency AlN Contour-Mode MEMS Resonators," *Electron Devices, IEEE Transactions on,* vol. 58, pp. 1281-1286, 2011.

[12] H. Campanella, *Acoustic Wave and Electromechanical Resonators: Concept to Key Applications*. Norwood,MA: Artech House, 2010.

[13] C. T. C. Nguyen, "MEMS technology for timing and frequency control," *Ultrasonics, Ferroelectrics and Frequency Control, IEEE Transactions on,* vol. 54, pp. 251-270, 2007.

[14] A. Rahafrooz and S. Pourkamali, "High-Frequency Thermally Actuated Electromechanical Resonators With Piezoresistive Readout," *Electron Devices,*

IEEE Transactions on, vol. 58, pp. 1205-1214, 2011.

[15] A. Rahafrooz*, et al.*, "Thermal actuation, a suitable mechanism for high frequency electromechanical resonators," in *Micro Electro Mechanical Systems (MEMS), 2010 IEEE 23rd International Conference on*, 2010, pp. 200-203.

[16] S. Pourkamali*, et al.*, "High-Q single crystal silicon HARPSS capacitive beam resonators with self-aligned sub-100-nm transduction gaps," *Microelectromechanical Systems, Journal of,* vol. 12, pp. 487-496, 2003.

[17] M. Akgul*, et al.*, "Hot filament CVD conductive microcrystalline diamond for high Q, high acoustic velocity micromechanical resonators," in *Frequency Control and the European Frequency and Time Forum (FCS), 2011 Joint Conference of the IEEE International*, 2011, pp. 1-6.

[18] W. Jing*, et al.*, "Self-aligned 1.14-GHz vibrating radial-mode disk resonators," in *TRANSDUCERS, Solid-State Sensors, Actuators and Microsystems, 12th International Conference on, 2003*, 2003, pp. 947-950 vol.2.

[19] M. U. Demirci*, et al.*, "Mechanically corner-coupled square microresonator array for reduced series motional resistance," in *TRANSDUCERS, Solid-State Sensors, Actuators and Microsystems, 12th International Conference on, 2003*, 2003, pp. 955-958 vol.2.

[20] S. Pourkamali*, et al.*, "Vertical capacitive SiBARs," in *Micro Electro Mechanical Systems, 2005. MEMS 2005. 18th IEEE International Conference on*, 2005, pp. 211-214.

[21] L. Yu-Wei*, et al.*, "Vibrating micromechanical resonators with solid dielectric capacitive transducer gaps," in *Frequency Control Symposium and Exposition,*

2005. Proceedings of the 2005 IEEE International, 2005, pp. 128-134.

[22] G. Piazza, "Integrated aluminum nitride piezoelectric microelectromechanical system for radio front ends," *Journal of Vacuum Science & Technology A: Vacuum, Surfaces, and Films,* vol. 27, pp. 776-784, 2009.

[23] G. Piazza*, et al.*, "Low motional resistance ring-shaped contour-mode aluminum nitride piezoelectric micromechanical resonators for UHF applications," in *Micro Electro Mechanical Systems, 2005. MEMS 2005. 18th IEEE International Conference on*, 2005, pp. 20-23.

[24] C. Brown*, et al.*, "Piezoelectric Materials, A Review of Progress," *Component Parts, IRE Transactions on,* vol. 9, pp. 193-211, 1962.

[25] G. K. Ho*, et al.*, "Piezoelectric-on-Silicon Lateral Bulk Acoustic Wave Micromechanical Resonators," *Microelectromechanical Systems, Journal of,* vol. 17, pp. 512-520, 2008.

[26] P. Wei*, et al.*, "High-tone bulk acoustic resonator integrated with surface micromachined FBAR filter on a single chip," in *Solid-State Sensors, Actuators and Microsystems, 2005. Digest of Technical Papers. TRANSDUCERS '05. The 13th International Conference on*, 2005, pp. 2057-2060 Vol. 2.

[27] G. Piazza*, et al.*, "AlN Contour-Mode Vibrating RF MEMS for Next Generation Wireless Communications," in *Solid-State Circuits Conference, 2006. ESSCIRC 2006. Proceedings of the 32nd European*, 2006, pp. 62-65.

[28] L. Khine*, et al.*, "Piezoelectric ALN MEMS resonators with high coupling coefficient," in *Solid-State Sensors, Actuators and Microsystems Conference (TRANSDUCERS), 2011 16th International*, 2011, pp. 526-529.

[29] G. Songbin*, et al.*, "A 1.75 GHz piezoelectrically-transduced SiC lateral overmoded bulk acoustic-wave resonator," in *Solid-State Sensors, Actuators and Microsystems Conference (TRANSDUCERS), 2011 16th International*, 2011, pp. 922-925.

[30] M. Shahmohammadi*, et al.*, "Concurrent enhancement of Q and power handling in multi-tether high-order extensional resonators," in *Microwave Symposium Digest (MTT), 2010 IEEE MTT-S International*, 2010, pp. 1452-1455.

[31] B. P. Harrington*, et al.*, "Toward ultimate performance in GHZ MEMS resonators: Low impedance and high Q," in *Micro Electro Mechanical Systems (MEMS), 2010 IEEE 23rd International Conference on*, 2010, pp. 707-710.

[32] B. P. H. a. R. Abdolvand, "In-plane acoustic reflectors for reducing effective anchor loss in lateral–extensional MEMS resonators " *Journal of Micromechanics and Microengineering,* vol. 21, 2011.

[33] R. Abdolvand, "Thin-Film Piezoelectric-on-Sunstrate Resonators and Narrowband Filters," Doctor of Philosophy, School of Electrical and Computer Engineering, Georgia Institute of Technology, 2008.

[34] J. D. Larson, III*, et al.*, "Modified Butterworth-Van Dyke circuit for FBAR resonators and automated measurement system," in *Ultrasonics Symposium, 2000 IEEE*, 2000, pp. 863-868 vol.1.

[35] G. Piazza*, et al.*, "One and Two Port Piezoelectric Contour-Mode MEMS Resonators for Frequency Synthesis," in *Solid-State Device Research Conference, 2006. ESSDERC 2006. Proceeding of the 36th European*, 2006, pp. 182-185.

[36] R. Abdolvand*, et al.*, "Thin-film piezoelectric-on-silicon resonators for high-

frequency reference oscillator applications," *Ultrasonics, Ferroelectrics and Frequency Control, IEEE Transactions on,* vol. 55, pp. 2596-2606, 2008.

[37] D. B. Leeson, "A simple model of feedback oscillator noise spectrum," *Proceedings of the IEEE,* vol. 54, pp. 329-330, 1966.

[38] L. Yu-Wei*, et al.*, "Low phase noise array-composite micromechanical wine-glass disk oscillator," in *Electron Devices Meeting, 2005. IEDM Technical Digest. IEEE International*, 2005, pp. 4 pp.-281.

[39] L. Seungbae and C. T. C. Nguyen, "Influence of automatic level control on micromechanical resonator oscillator phase noise," in *Frequency Control Symposium and PDA Exhibition Jointly with the 17th European Frequency and Time Forum, 2003. Proceedings of the 2003 IEEE International*, 2003, pp. 341-349.

[40] Z. Chengjie*, et al.*, "Dual-Mode Resonator and Switchless Reconfigurable Oscillator Based on Piezoelectric AlN MEMS Technology," *Electron Devices, IEEE Transactions on,* vol. 58, pp. 3599-3603, 2011.

[41] V. Kaajakari*, et al.*, "Low noise silicon micromechanical bulk acoustic wave oscillator," in *Ultrasonics Symposium, 2005 IEEE*, 2005, pp. 1299-1302.

[42] R. Abdolvand*, et al.*, "Single-Resonator Dual-Frequency Thin-Film Piezoelectric-on-Substrate Oscillator," in *Electron Devices Meeting, 2007. IEDM 2007. IEEE International*, 2007, pp. 419-422.

[43] S. Smith, *Microelectronic Circuit*, 5th ed.: Oxford University Press, USA; 5 Har/Cdr edition, 2007.

[44] T. Wong and M. Palaniapan, "Micromechanical oscillator circuits: theory and

analysis," *Analog Integrated Circuits and Signal Processing,* vol. 59, pp. 21-30, 2009.

[45] Y. Tsuzuki*, et al.*, "Formulation of nonlinear negative resistance for calculation of start-up characteristics of crystal oscillators," in *Frequency Control Symposium, 1996. 50th., Proceedings of the 1996 IEEE International.*, 1996, pp. 710-713.

[46] C. Ying*, et al.*, "A Novel Technique to Enhance the Negative Resistance for Colpitts Oscillators by Parasitic Cancellation," in *Electron Devices and Solid-State Circuits, 2007. EDSSC 2007. IEEE Conference on*, 2007, pp. 425-428.

[47] J. Matsuoka*, et al.*, "A circuit for high frequency crystal oscillators," in *Frequency Control Symposium and PDA Exhibition Jointly with the 17th European Frequency and Time Forum, 2003. Proceedings of the 2003 IEEE International*, 2003, pp. 569-574.

[48] N. Nomura*, et al.*, "1 [GHz] high frequency Colpitts oscillator," in *Frequency Control Symposium and Exposition, 2005. Proceedings of the 2005 IEEE International*, 2005, p. 4 pp.

[49] N. Norio*, et al.*, "A Colpitts-Type Crystal Oscillator for Gigahertz Frequency," in *International Frequency Control Symposium and Exposition, 2006 IEEE*, 2006, pp. 233-236.

[50] Y. Chen and K. Mouthaan, "Design of dual-band colpitts VCO by switched negative resistance shaping," *Microwave and Optical Technology Letters,* vol. 53, pp. 1356-1360, 2011.

[51] H. Packard, "S-parameter technique."

[52] R. K.Poorfard, "Phase Noise Analysis and Measurement," Silicon Laboratories

Inc.April 2005.

[53] R. Poore, "Phase Noise And Jitter," Agilent EEsof EDA2001.

VITA

Derya Dikbas

Candidate for the Degree of

Master of Science

Thesis: THIN FILM PIEZOELECTRIC ON SUBSTRATE RESONATORS ELECTRICAL CHARACTERIZATION AND OSCILLATOR CIRCUIT DESIGN

Major Field: Electrical Engineering

Education:

Completed the requirements for the Master of Science in Electrical Engineering at Oklahoma State University, Stillwater, Oklahoma in December, 2011.

Completed the requirements for the Bachelor of Science in Electrical Engineering at Yildiz Technical University, Istanbul, Turkey, in 2009.

Experience:

Research Assistant, Microsystems Laboratory January 2010-December 2011
Oklahoma State University, Tulsa,Oklahoma
Department of Electrical Engineering

Professional Memberships: IEEE

Name: Derya Dikbas Date of Degree: December, 2011

Institution: Oklahoma State University Location: Stillwater, Oklahoma

Title of Study: THIN FILM PIEZOELECTRIC ON SUBSTRATE RESONATORS ELECTRICAL CHARACTERIZATION AND OSCILLATOR CIRCUIT DESIGN

Pages in Study: 73 Candidate for the Degree of Master of Science

Major Field: Electrical Engineering

Scope and Method of Study:

In the present work, resonant behavior of TPoS resonator is studied with their electrical equivalent circuit model. Equivalent circuit model parameters are extracted for one-port and two-port configuration of TPoS. The effects of perforated and continuous electrode designs on resonant behavior are investigated. The extracted TPoS resonator model is used for oscillator simulation model. The colpitts oscillator circuit is implemented on a PC Board with the TPoS resonant device and quartz resonant device.

Findings and Conclusions:

The resonant behavior of the TPoS resonator is influenced by design aspects. It is observed that the resonance frequency shifts downward with the perforated electrode design for identical devices. An interesting finding was that contrast resonance behavior was observed for 54 MHz and 27 MHz devices. The quality factor and the insertion loss were improved for 27 MHz devices with the perforated electrode design. However, a higher insertion loss and lower quality factor is measured for 54 MHz devices with perforated design. Moreover, the lower quality factor and higher motional resistance were noted for larger hole area within identical perforated designs. Quality factor of the TPoS increases with the increased substrate thickness.

TPoS resonator and quartz resonator were used to build colpitts oscillator circuit. A modified colpitts oscillator is used with a collector inductor and an emitter inductor. The circuit model is designed in Multisim with extracted parameters of 27 MHz TPoS resonator. The circuit is tested with quartz resonator and TPoS resonator. Lower jitter (8.6ps) is measured with TPoS resonator for this particular circuit.

ADVISER'S APPROVAL: Dr. Reza Abdolvand